Dynamics of histone H3.3 deposition in proliferating and senescent cells reveals a DAXX-dependent targeting to PML-NBs important for pericentromeric heterochromatin organization

Corpet, Armelle ; Olbrich, Teresa ; Gwerder, Myriam ; Fink, Daniel ; Stucki, Manuel

Abstract: Oncogene-induced senescence is a permanent cell cycle arrest characterized by extensive chromatin reorganization. Here, we investigated the specific targeting and dynamics of histone H3 variants in human primary senescent cells. We show that newly synthesized epitope-tagged H3.3 is incorporated in senescent cells but does not accumulate in senescence-associated heterochromatin foci (SAHF). Instead, we observe that new H3.3 colocalizes with its specific histone chaperones within the promyelocytic leukemia nuclear bodies (PML-NBs) and is targeted to PML-NBs in a DAXX-dependent manner both in proliferating and senescent cells. We further show that overexpression of DAXX enhances targeting of H3.3 in large PML-NBs devoid of transcriptional activity and promotes the accumulation of HP1, independently of H3K9me3. Loss of H3.3 from pericentromeric heterochromatin upon DAXX or PML depletion suggests that the targeting of H3.3 to PML-NBs is implicated in pericentromeric heterochromatin organization. Together, our results underline the importance of the replication-independent chromatin assembly pathway for histone replacement in non-dividing senescent cells and establish PML-NBs as important regulatory sites for the incorporation of new H3.3 into chromatin.

DOI: https://doi.org/10.4161/cc.26988

Dynamics of histone H3.3 deposition in proliferating and senescent cells reveals a DAXX-dependent targeting to PML-NBs important for pericentromeric heterochromatin organization

(Title: 177 characters)

Authors:

Armelle CORPET*, Teresa OLBRICH, Myriam GWERDER, Daniel FINK and Manuel STUCKI*

Affiliation:

University Hospital Zürich, Departement of Gynecology, Wagistrasse 14, 8952 Schlieren, Switzerland.

* Corresponding authors:

Armelle Corpet: armelle.corpet@usz.ch, +41 44 556 30 46.

Manuel Stucki: manuel.stucki@usz.ch, +41 44 556 30 40.

Keywords: chromatin dynamics, H3.3, DAXX, senescence, PML-NBs

List of abbreviations and acronyms:

ATRX: alpha-thalassemia mental retardation X-linked

DAXX: death-domain associated protein

HP1: heterochromatin protein 1

OIS: oncogene-induced senescence

PML: promyelocytic leukemia

PML-NBs: PML nuclear bodies

SAHF: senescence associated heterochromatin foci

Abstract

Oncogene-induced senescence is a permanent cell cycle arrest characterized by extensive chromatin reorganization. Here, we investigated the specific targeting and dynamics of histone H3 variants in human primary senescent cells. We show that newly synthesized epitope-tagged H3.3 is incorporated in senescent cells but does not accumulate in senescence-associated heterochromatin foci (SAHF). Instead, we observe that new H3.3 colocalizes with its specific histone chaperones within the promyelocytic leukemia nuclear bodies (PML-NBs) and is targeted to PML-NBs in a DAXX-dependent manner both in proliferating and senescent cells. We further show that overexpression of DAXX enhances targeting of H3.3 in large PML-NBs devoid of transcriptional activity and promotes the accumulation of HP1, independently of H3K9me3. Loss of H3.3 from pericentromeric heterochromatin upon DAXX or PML depletion suggests that the targeting of H3.3 to PML-NBs is implicated in pericentromeric heterochromatin organization. Together, our results underline the importance of the replication-independent chromatin assembly pathway for histone replacement in non-dividing senescent cells and establish PML-NBs as important regulatory sites for the incorporation of new H3.3 into chromatin.

Introduction

Most mammalian cells only divide for a limited number of times before they undergo terminal differentiation or enter the state of senescence. Cellular senescence may be triggered by various forms of stress stimuli. First described as the result of replicative exhaustion of cultured normal diploid cells [1], senescence can also be induced by oxidative stress, activated oncogenes such as H-RasV12 or inadequate growth conditions [2,3,4,5]. Oncogene-induced senescence (OIS) results from a DNA damage response (DDR) activated by aberrant DNA replication [6,7,8] and may pose as an important anti-tumor barrier. Identification of senescent cells in benign or premalignant, but not malignant tissues or using various human and mouse model systems seems to support this hypothesis [9,10,11,12,13]. Like terminal differentiation, senescence is characterized by irreversible cell cycle arrest and rigorous reorganization of cellular morphology, including the structure of the chromatin.

Chromatin is comprised of nucleosomes that each consists of 147 base pairs of DNA wrapped around a core histone octamer. The histone octamer is composed of a central $(H3\text{-}H4)_2$ tetramer flanked by two H2A-H2B histone dimers [14]. Three principle mechanisms bring about chromatin alterations in eukaryotic cells: i) post-translational modification of histone tails, ii) the action of chromatin remodeling enzymes and iii) the replacement of canonical histone proteins by histone variants [14]. Incorporation of histone variants into chromatin is orchestrated by a family of proteins called histone chaperones [15] and may provide different biophysical properties to the chromatin fiber or different post-translational modification sites thus influencing nucleosome stability and function [14,16].

Histone H3.3 is a variant of histone H3 that differs by only 5 amino acids from the canonical replicative histone variant H3.1 and has emerged as a regulator of chromatin states [17]. H3.3 is constitutively expressed throughout the cell cycle and in quiescence [18] and is incorporated into chromatin in a DNA-synthesis-independent manner [19,20]. It is enriched within actively

transcribed genes [21,22,23,24,25], but also accumulates at pericentromeric and telomeric heterochromatin regions [26,27,28]. While the histone chaperone HIRA along with associated factors, ASF1a, Ubinuclein1 and Cabin1, is responsible for H3.3 deposition into active chromatin [19,20,27,29,30,31,32], the H3.3-specific chaperone DAXX in cooperation with the chromatin remodeler ATRX is essential for H3.3 deposition at heterochromatic loci [26,27,33]. The ATRX/DAXX/H3.3 pathway has been implicated in the suppression of pancreatic neuroendocrine tumors (panNET) and paediatric glioblastomas [34,35,36,37,38,39] thus establishing its role in carcinogenesis.

While establishment and maintenance of chromatin structure is central for genome function [40], how such a mechanism is achieved in senescent cells has remained unclear. Chromatin structure is extensively remodeled upon senescence entry as exemplified by the formation of senescence-associated heterochromatin foci (SAHF), visible as microscopically discernible, punctate DNA foci in DAPI-stained senescent cells [41]. These structures are thought to contribute to the senescence-associated cell-cycle arrest in part by silencing proliferation-promoting genes through heterochromatinization [41]. Moreover, oncogene-induced SAHF formation may protect premalignant cells to undergo apoptosis by limiting extensive DNA damage to sub-lethal levels [42].

Little is known about the underlying mechanisms of the extensive chromatin reorganization observed in senescent cells. SAHF are enriched in markers of heterochromatin including tri-methylated histone H3 at lysine 9 (H3K9me3), all HP1 isoforms as well as HMGA proteins [41,43]. In addition, SAHF are also enriched in the histone H2A variant macroH2A [44], a variant associated with gene silencing as for example during X inactivation [45]. Formation of MacroH2A- and HP1-containing SAHF is dependent on the two histone chaperones HIRA and ASF1a [44], suggesting that H3.3 may become enriched in SAHF during OIS [44,46]. Interestingly, SAHF formation also depends on the prior localization of HIRA into

promyelocytic leukemia (PML) nuclear bodies (PML-NBs) [44,47], descrete foci, 0.2-1.0μm wide, that are present in most mammalian cell nuclei and stain positive for the tumor suppressor PML [48,49]. PML-NBs have previously been implicated in the onset of OIS: they increase in number and size upon overexpression of H-RasV12 and overexpression of PML triggers p53-dependent senescence [50,51]. Thus, PML-NBs may represent important regulatory structures not only for the induction of OIS in general but also for the establishment and maintenance of the specialized chromatin structure characteristic of the senescent state.

In this study we set out to investigate the dynamics of H3.3 incorporation in senescent cells, and in particular its possible connection with PML-NBs. To this end we employed the novel SNAP-tagging approach, which has been successfully used to investigate the deposition of newly synthesized H3 variants in human cells [20,52]. Surprisingly, we show here that H3.3 is not enriched in SAHF. Instead, we find that H3.3 is incorporated in active chromatin regions during senescence. In addition, we also observe the DAXX-dependent recruitment of H3.3 into PML-NBs both in proliferating and senescent cells, thus establishing PML-NBs as important assembly points for newly synthesized H3.3 histones. We further show a decrease in the localization of H3.3 to satellite DNA regions upon depletion of DAXX or PML in human primary cells, thus linking the targeting of H3.3 to PML-NBs with the maintenance of pericentromeric heterochromatin.

Results

An *in vivo* visualisation assay for newly synthesized H3.1 and H3.3 deposition in primary cells

In order to address the dynamics of the histone variants H3.1 and H3.3 in proliferating and senescent cells, we established human MRC5 primary diploid fibroblasts stably expressing H3.1 or H3.3 tagged with SNAP and three HA epitopes (MRC5 e-H3.1 and e-H3.3, respectively). SNAP is a modified variant of a suicide DNA repair enzyme that catalyzes its own irreversible covalent binding to the cell-permeable molecule benzylguanine (BG). For *in vivo* labeling assays BG is replaced by fluorescent or non-fluorescent derivatives [53,54]. This technique is tailor-made to visualize proteins synthesized at different time points, thus permitting to distinguish between old histone proteins and newly synthesized ones [20,52,54] **(Suppl. Fig. S1A)**. In particular, this system prooved essential to address the incorporation and localization of new histones in senescent cells, because in regular epitope-tagged H3 expressing cell lines, it would be impossible to distinguish between incorporation of new histones versus chromatin-wide incorporation of H3 after senescence induction.

We first verified by immunofluorescent staining that the tagged histones colocalize with mitotic chromosomes, indicating that the presence of the epitope tag does not interfere with the deposition of H3.1 nor H3.3 into chromatin *in vivo* **(Suppl. Fig. S1B)**. We then validated in both cell lines the efficiency of our *in vivo* deposition assay based on quench-chase-pulse (QCP) labeling. Microscopic analysis shows that the pulse with TMR-Star labeled both pre-existing H3.1 and H3.3 efficiently. In contrast, although pre-existing histones could still be labeled with HA antibody, a quench-pulse assay only gave background staining confirming the efficiency of quenching. A chase period during which new histone biosynthesis takes place then allowed the selective labelling of the new histones with TMR-Star **(Fig. 1A and**

Suppl. Fig. S1A-C). Furthermore, by combining quench-chase-pulse labeling assay with BrdU incorporation to detect replicating cells we confirmed that H3.1 deposition is limited to S-phase while H3.3 deposition occurs throughout the cell cycle **(Suppl. Fig. S1B-D)** [20]. We conclude that human primary MRC5 cell lines expressing SNAP-HAx3-tagged histones are a powerful tool to analyse the mechanisms of *de novo* deposition of H3.1 and H3.3 at the single-cell level.

Newly synthesized H3.3 is actively deposited in senescent cells while H3.1 is not

To analyse the deposition of H3.1 and H3.3 variants in senescent cells, we induced senescence in MRC5 human primary diploid cells by overexpression of oncogenic Ras using retroviral-mediated gene transfer. At 8 days post-infection, MRC5 cells had arrested at sub-confluent density, displayed reduced BrdU incorporation and showed the characteristic formation of SAHF visible as DAPI-dense foci, as described previously **(Suppl. Fig. S2A,C)** [4,41]. In addition, MRC5 cells also stained positive for the senescence-associated β-galactosidase [55,56] thus confirming the entry into senescence **(Suppl. Fig. S2B-C)**. We then overexpressed oncogenic Ras to induce senescence in MRC5 e-H3.1 or e-H3.3 cells **(Fig. 1B)** and performed quench-chase-pulse experiments to followed new histone deposition into chromatin. We verified that the newly synthesized histones are incorporated into chromatin by performing a detergent extraction to remove soluble histones prior to fixation of the cells **(Suppl. Fig. S2D)**. Newly deposited H3.1 was detected in about 24% of proliferating cells **(Fig. 1C-D)**, corresponding to S-phase cells **(Suppl. Fig. S1C-D),** consistent with previous work [19,20]. In contrast, new H3.1 was not incorporated in senescent cells even though we could still detect the pool of pre-existing histones H3.1 by HA staining **(Fig. 1C)**. Interestingly, pre-existing e-H3.1 accumulated at SAHF regions, marked as H3K9me3/ DAPI-dense foci, possibly as a result of the high condensation of these heterochromatin

regions **(Fig. 2A-B)**. We next examined the deposition of new H3.3 in proliferating primary cells and confirmed its incorporation throughout the cell cycle in about 85% of cells. This number did not reach 100% because a certain percentage of cells expressed very low levels of recombinant histones, which resulted in undetectable TMR-star signal. Importantly, we could show for the first time *de novo* deposition of new H3.3 in senescent cells **(Fig. 1C-D)**. Quantification of the number of TMR positive cells in Ras-arrested cells revealed that almost all senescent cells incorporated new H3.3 **(Fig. 1D).** Of note, endogenous H3.3 is still efficiently expressed in senescent cells (at about 60% of its levels in proliferating cells) as seen by quantitative PCR, as compared to a reduction to about 35% for H3.1 **(Suppl. Fig. S3A-B)** underscoring the importance to maintain a pool of H3.3 histones during senescence. Thus, our results suggest that replication-independent nucleosome assembly is the predominant mode of histone replacement in senescent cells.

Newly synthesized H3.3 deposition in senescent cells correlates with active transcription

We then decided to examine more closely where exactly newly synthesized H3.3 is deposited in senescent cells. Given the difficulty to specifically detect endogenous H3 variants by microscopy (H3.1 and H3.3 differ in only five amino acids), it has not yet been possible to determine the histone H3 variant composition of SAHF. These foci were originally described as transcriptionally inactive heterochromatin on the basis of the presence of all HP1 isoforms as well as H3K9me3 by immunofluorescence analysis [41,44]. We first set out to confirm the transcriptionally silent state of SAHF. By combining immunostaining of H3K9me3 to detect SAHF with 5-Ethynyl uridine (EU) to label global nascent RNA transcription *in vivo*, we observed that EU labeling was clearly excluded from SAHF, marked as H3K9me3/ DAPI-dense foci **(Fig. 2C)**. We quantified fluorescent intensity profiles along a line drawn through the centers of the nuclei of senescent cells and confirmed the inverse correlation between *de*

novo RNA synthesis and SAHF presence in MRC5 senescent cells **(Fig. 2D)**. Thus, our results substantiate the transcriptionally silent state of the SAHF regions.

Importantly, SAHF formation is in part regulated by the H3.3 histone chaperones HIRA and ASF1a [44,47], suggesting involvment of the H3.3 histone variant in this process. We thus investigated if new H3.3 becomes incorporated in SAHF by using our powerful *in vivo* deposition assay. We combined a quench-chase-pulse labelling of new H3.3 by TMR-star with H3K9me3 immunostaining as a marker of SAHF. We observed no enrichment of new H3.3 at H3K9me3/DAPI dense foci **(Fig. 2E)**, confirmed by the striking reverse correlation of fluorescent intensity profiles of new H3.3 (TMR) and SAHF (H3K9me3 and DAPI-dense peaks) **(Fig. 2F)**, reminiscent of the profiles observed with EU labelling. Confocal microscopy confirmed the absence of new H3.3 within SAHF in single plane images **(Suppl. Fig. S3C)** thus strongly indicating that most incorporation of new H3.3 in senescent cells takes place at transcriptionally active regions of the nucleus. While epitope-tagging can sometimes interfere with the function of the protein, we also extended these experiments to endogenous H3.3 by using a specific H3.3 antibody [26] for immunofluorescence analysis in IMR90 ER:Ras primary fibroblasts driven into senescence with addition of 4-hydroxytamoxifen (4-OHT) [57] **(Suppl. Fig. S3D)**. While the endogenous H3.3 behaved similarly to SNAP-HA-tagged recombinant H3.3, our data do not exclude the possibility that H3.3 could also be deposited in specific heterochromatic regions outside of SAHF.

Newly synthesized H3.3 localizes in PML-NBs together with DAXX and ATRX in proliferating and senescent cells

We next inspected more closely H3.3 labeling patterns in senescent cells. Remarkably, we noticed a distinct intranuclear focal H3.3 staining in the vast majority of cells, but not in MRC5 e-H3.1 cells, suggesting a distinct chromatin assembly pathway for H3.1 and H3.3.

Interestingly, the distinct nuclear H3.3 foci were also present in proliferating cells, although they were smaller in size and intensity as compared to senescent cells, reminiscent of the pattern observed for PML-NBs [50,51]. We thus wondered if these H3.3 foci would co-localize with PML-NBs, together with its specific chaperones DAXX, ATRX, HIRA and ASF1a. Combined quench-chase-pulse labeling of new H3.3 by TMR-star with PML and DAXX/ATRX triple immunostaining clearly revealed that H3.3 co-localizes with PML-NBs in both proliferating and oncogene-induced senescent cells together with its associated histone chaperones DAXX and ATRX **(Fig. 3A,C)**. We confirmed these data by fluorescent intensity profiles drawn through nuclei **(Fig. 3B, D)**. We extended our results obtained on e-H3.3 to the endogenous histone H3.3 and showed its localization at PML-NBs both in proliferating and senescent human primary fibroblasts **(Suppl. Fig. S4A)**. We also observed increased size and intensities of DAXX, ATRX, and new H3.3 foci in senescent cells **(Figure 3 and Suppl. Fig. S4A)** as demonstrated previously for PML-NBs [50,51]. In addition, new H3.3 also co-localized with HIRA and ASF1a **(Suppl. Fig. S4B)**.

H3.3 interacts with DAXX and ATRX in proliferating cells [26,27,33]. Hence, the strong co-localization of e-H3.3 with DAXX and ATRX in PML-NBs in senescent cells prompted us to analyse the interaction of H3.3 with its chaperones in senescent cells. We first confirmed by western blot analysis of fractionated cell extracts that H3.3 as well as all H3.3 chaperones remain expressed in senescent MRC5 cells **(Suppl. Fig. S3B)**, in contrast to the proliferative marker MCM7 or to the H3.1 histone chaperone CAF-1 [58]. We then purified histone complexes by HA immunoprecipitation in nuclear extracts from senescent MRC5 e-H3.1- and e-H3.3- expressing cells lines. Immunoblotting analysis of the purified complexes revealed the specific presence of DAXX and ATRX in H3.3 complexes but not of H3.1 in senescent cells **(Fig. 3E)** thus corroborating their function in H3.3 dynamics during senescence.

Interestingly, before the function of DAXX and ATRX in histone H3.3 chromatin assembly

was identified, both factors were known to be components of PML-NBs in proliferating cells [59,60] raising the possibility that these chaperones could localize in PML-NBs during senescence to regulate replication-independent chromatin assembly. We thus sought to verify the localization of these H3.3 chaperones as well as HIRA and ASF1a in PML-NBs in absence of H3.3 overexpression. While only a subpopulation of cells showed HIRA and ASF1a at PML-NBs in proliferating cells, this number increased upon senescence, as described previously [44,61]. In contrast, ATRX and DAXX co-localized each in PML-NBs in almost all proliferating and senescent cells **(Suppl. Fig. S4C)**. In addition, focal staining of all histone chaperones showed an increase in size and intensity in senescent cells, consistent with the pattern observed for PML-NBs [50,51]. Of note, ATRX also localized to a fraction of SAHF in senescent cells, in addition to its localization to PML-NBs (**Suppl. Fig. S4C** and **S9H**). Together, our results indicate that new H3.3 localizes to PML-NBs together with its associated chaperones, and that this occurs in an increased manner during senescence.

DAXX-dependent recruitment of H3.3 to PML-NBs

We next made use of our *in vivo* deposition assay to directly assess the role of histone chaperones in targeting of H3.3 to PML-NBs both in proliferating and senescent cells. Co-localization of DAXX and ATRX with new H3.3 at PML-NBs and their interaction with H3.3 in both proliferating and senescent cells **(Fig. 3)** suggested that either chaperone could mediate H3.3 targeting to PML-NBs. To test this, we depleted DAXX and ATRX by RNA interference in MRC5 cells and first checked the efficiency of the knockdown by western blot analysis and ensured that depletion of each chaperone does not affect levels of the other **(Suppl. Fig. S5A)**. Strikingly, specific depletion of DAXX with two different siRNAs, but not of HIRA nor H3.3, led to a dramatic loss of ATRX from the PML-NBs **(Suppl. Fig. S5B)** [60] and was accompanied by a striking increase of ATRX localization at SAHF in Ras-induced

cells **(Suppl. Fig. S6A-B)**. In contrast, downregulation of ATRX, HIRA or H3.3 did not affect DAXX localization in PML-NBs **(Suppl. Fig. S5B)**. Thus, ATRX localization in PML-NBs is DAXX-dependent.

We then assessed the localization of newly synthesized H3.3 in PML-NBs in absence of DAXX or ATRX. To this end we first transduced MRC5 cells expressing e-H3.3 with empty vector or oncogenic Ras-expressing viruses followed by DAXX or ATRX depletion **(Fig. 4A)**. Efficient downregulation of the H3.3 chaperones and expression of oncogenic Ras were verified by western blot analysis **(Fig. 4B)**. We observed a dramatic loss of new H3.3 histones at PML-NBs upon DAXX depletion with two different sets of siRNAs, both in proliferating and in senescent cells **(Fig. 4C)**, confirmed by quantification **(Fig. 4D)**. As a control, PML depletion also led to a loss of H3.3 at PML-NBs **(Suppl. Fig. S7A-C).** In contrast, neither knockdown of ATRX **(Fig. 4C-D)** nor HIRA **(Suppl. Fig. S7D-F)** affected H3.3 localization at PML-NBs. Thus, our results reveal that DAXX promotes H3.3 recruitment to PML-NBs in proliferating and senescent cells.

Given the essential role of PML in the induction of senescence through p53 activation and regulation of SAHF formation [44,50,51], we wondered if DAXX, ATRX or H3.3 depletion would impair Ras-induced senescence. We used two strategies to deplete DAXX and ATRX by shRNA. We either cotransduced MRC5 human primary fibroblasts with viruses encoding oncogenic Ras and the specific shRNA or we used IMR90 ER:Ras transduced with shRNAs 5 days before induction of senescence by addition of 4-OHT. In both cases, we could not detect any defects in SAHF formation or senescence entry **(Suppl. Fig. S8A-C and Suppl. Fig. S9A-E)**. Of note, overexpression of DAXX did not affect oncogene-induced senescence either because we observed normal reduction in Cyclin A levels, increase in p16 expression and normal SAHF formation in MRC5 and IMR90 ER:Ras overexpressing DAXX and the oncogenic form of Ras **(Suppl. Fig. S8D-E and Suppl. Fig. S9E)**. In addition, we also

depleted DAXX, ATRX and H3.3 by siRNA in IMR90 ER:Ras one day before the induction of senescence. After 6 days of 4-OHT and 2 rounds of siRNA transfection to ensure continuous knock-down of the proteins, we could not detect any defects in senescence entry in DAXX- ATRX- and H3.3-depleted cells **(Suppl. Fig. S9F-H)**. Thus, we decided to pursue our analysis in proliferating cells in order to investigate further the possible functions of H3.3 localization in PML-NBs.

DAXX overexpression increases localization of H3.3 at PML-NBs

We first asked if overexpression of DAXX protein would trigger the reverse phenotype as observed upon DAXX depletion. We therefore transduced MRC5 e-H3.3 cells with retroviruses encoding Myc-DAXX. Upon overexpression of DAXX, triple immunostaining analysis showed perfect colocalization of new H3.3 with Myc-DAXX in PML-NBs along with a marked increase of the H3.3 signal within PML-NBs **(Fig. 5A-B)**, sometimes leading to a massive accumulation of new H3.3 in a very large single PML-NB surrounded by a thin spherical enrichment of PML and DAXX proteins **(Suppl. Fig. S10A).** We then assessed if overexpression of recombinant DAXX could rescue the loss of H3.3 at PML-NBs in proliferating cells that were depleted from endogenous DAXX. To this end, we generated a siRNA-resistant derivative of Myc-DAXX by inserting silent mutations in the siRNA-target region and verified that it is not targeted by the siDAXX1 **(Fig. 5B)**. Quench-chase-pulse labelling assays in MRC5 e-H3.3 cells depleted of endogenous DAXX showed that overexpression of Myc-DAXX rescues the localization of H3.3 in PML-NBs **(Fig. 5C-D)** and even leads to an increased H3.3 recruitment to PML-NBs, similar to the results obtained after overexpression of DAXX **(Fig. 5A)**. Together, our results underline the essential role of DAXX for the recruitment of H3.3 to PML-NBs and rule out an off-target effect of our DAXX siRNA.

PML-NBs are not sites of H3.3 deposition but rather serve as interstages in the chromatin assembly pathway of H3.3

While the precise roles of PML-NBs remains elusive, it was proposed that PML-NBs may serve as sites of storage for proteins or could be active sites for transcriptional and chromatin regulation [48]. Importantly, in our analysis we observed that both the pools of soluble **(Fig. 3A-D)** and incorporated new H3.3 (histones resistant to detergent extraction, **Suppl. Fig. S10B**) localize in PML-NBs, suggesting incorporation of H3.3 into chromatin within the PML-NBs. Given the non-random association of PML-NBs with transcriptionally active regions [62,63] and the importance of the histone variant H3.3 for transcriptional activation [17], we first tested if PML-NBs could be direct sites of H3.3 assembly during transcription. We took advantage of MRC5 cells overexpressing Myc-DAXX, which feature large PML-NBs (as observed in **Fig. 5A**) that contain DAXX and are surrounded by a thin PML "shell" **(Fig. 6A-B)**. We combined immunostaining of Myc and PML with 5-Ethynyl uridine (EU) to detect localization of the epitope-tagged DAXX proteins within the large PML-NBs and ongoing RNA transcription *in vivo*. We observed a striking exclusion of *de novo* RNA synthesis within the shell formed by PML proteins in the large PML-NBs **(Fig. 6C)** suggesting that PML-NBs do not contain any detectable nascent RNA. Of note, we also noticed a low DAPI intensity at the place of the large PML-NBs **(Fig. 6C-D**, **Suppl. Fig. S10A**) suggesting absence or low DNA content in these structures, consistent with previous work [64]. In addition, we observed that new H3.3 still localizes to PML-NBs upon transcription inhibition with Actinomycin D in proliferating and senescent cells **(Suppl. Fig. S11A-B)**. Thus, PML-NBs are unlikely to be direct sites of chromatin incorporation for H3.3 and may rather function as storage bodies or indirectly regulate chromatin assembly pathways. Given the physical association of H3.3 with several histone chaperones within PML-NBs **(Fig.**

3, Suppl. Fig. S4B), we hypothesized that PML-NBs could be gathering points in the replication-independent chromatin assembly pathway for H3.3 before its deposition in specific genomic locations.

H3.3 is targeted to pericentromeric heterochromatin in a DAXX- and PML-dependent manner

To test this hypothesis, we focused on pericentromeric heterochromatin, a typical form of constitutive heterochromatin that is crucial for proper chromosome segregation. It is composed of DNA satellite repeats packed in heterochromatin that is associated with specific histone modifications such as H3K9me3 and is enriched in HP1 proteins [65]. Interestingly, H3.3 was recently shown to be enriched in pericentromeric heterochromatin in mouse cells [26] as well as in human cells [66]. We first asked if PML-NBs contain pericentromeric heterochromatin markers. Thus, we performed immunofluorescence staining against HP1γ or H3K9me3 in MRC5 cells overexpressing Myc-DAXX. We observed a striking accumulation of HP1γ in the core of the large PML-NBs, but no local increase in H3K9me3 modification **(Fig. 6D-E)**, suggesting the presence of a soluble pool of HP1 proteins within the PML-NBs. Of note, concentration of HP1γ into the large prominent nuclear body was not dependent on transcription or on any RNA component as it persisted in cells treated with Actinomycin D and RNaseA, respectively (data not shown).

We then used chromatin immunoprecipitation (ChIP) to assess the localization of H3.3 histones in our human primary MRC5 e-H3.3 stable cell lines. In normal MRC5 e-H3.3 cells, H3.3 localizes to the promoter of the active house-keeping gene GAPDH, as well as to centromeric (α-Satellite) and pericentromeric heterochromatin regions (Satellite III) **(Fig. 7A)**. Upon depletion of DAXX by siRNA transfection **(Fig. 7C)**, we observed a slight reduction of H3.3 localization at α-satellite regions and a much more prononced reduction at

pericentromeric heterochromatin (about 50% reduction) **(Fig. 7A)**, whereas H3.3 localization at the GAPDH promoter was unaffected **(Fig. 7B)**. Importantly, and in contrast to DAXX depletion, depletion of PML led to a marked decrease in the localization of H3.3 at both centromeric and pericentromeric heterochromatin **(Fig. 7A)**, and also at the GAPDH promoter **(Fig. 7B)**. These results suggest that depletion of PML (and disruption of PML-NBs) impairs H3.3 deposition at specific genomic locations both in euchromatin and heterochromatin. We next asked if DAXX-mediated targeting of H3.3 to pericentromeric heterochromatin via the PML-NB route would affect the levels of transcription of this region. To this end, we measured the levels of RNA transcripts for the satellite III region by qRT-PCR. In normal MRC5 cells, the level of Satellite III transcripts was below the detection limit, thus preventing us from studying a possible decrease in transcription upon DAXX knock-down. However, upon DAXX overexpression, we observed increased levels of Satellite III transcripts as measured by quantitative RT-PCR **(Fig. 7D)**. We thus wondered if this increase was associated with an enhanced localization of H3.3 at the satellite III region. We performed ChIP against H3.3 histones in MRC5 e-H3.3 cells overexpressing Myc-DAXX. In comparison with empty MRC5 e-H3.3 cells, H3.3 localization to α-satellite regions was slighly increased, and a pronounced increase was observed at pericentromeric heterochromatin upon DAXX overexpression **(Fig. 7E)**. H3.3 localization at the GAPDH promoter remained unaltered **(Fig. 7F)**. Together, our results implicate PML-NBs in the histone H3.3 assembly process and support a model in which PML-NBs may play an important role for chromatin organization at specific genomic locations such as pericentromeric heterochromatin.

Discussion

Our comprehensive analysis of H3.1 and H3.3 deposition *in vivo* provides novel insights into the dynamics of these H3 variants and their chromatin-assembly pathways in proliferating and senescent primary human cells. We show a global incorporation of new H3.3 in senescent cells with no accumulation into SAHF but instead localization in PML-NBs together with its known chaperones ASF1a, HIRA, DAXX and ATRX. We further demonstrate a specific role of DAXX in the targeting of H3.3 to PML-NBs in proliferating and senescent cells and we present evidence that this process is important for pericentromeric heterochromatin organization. Together, our results results implicate PML-NBs in the replication-independent chromatin assembly pathway of H3.3.

Replication-independent chromatin assembly as a source of histone replacement in senescent cells

While chromatin structure is inherently dynamic [67], the question of how chromatin is maintained in the absence of DNA replication has remained elusive. In particular, persistance of senescent melanocytes in benign human naevi in the human body for decades [9] highlights the need for chromatin maintenance mechanisms to secure the senescent phenotype. Whereas a global increase in protein content, as well as a specific increase in the macroH2A histone variant has been reported in senescence [44,68], a decrease in the protein levels of the histones H2A, H3 and H4 was described upon drug-evoked senescence or replicative aging [69,70] suggesting that chromatin destabilization is associated with senescence. Here, we extend these results by reporting a dramatic decrease in H3.1 mRNA levels and a mild reduction of H3.3 mRNA levels in OIS **(Suppl. Fig. S3A)**. In addition, by taking advantage of the SNAP-tagging technology to label new histones in human primary cells, we report that new H3.3 but not H3.1 is incorporated in senescent cells. While this result is not surprising given the

downregulation of the H3.1- specific histone chaperone CAF-1 in non-dividing cells [58,71], deposition of H3.3 in senescent cells suggests that replication-independent chromatin assembly is an important mode of histone replacement in non-dividing senescent cells. Recent studies identifying driver H3.3 mutations in pediatric glioblastomas [34,35,36,37], or linking H3.3 incorporation with cellular memory [72], further underscore the physiological importance of H3.3 deposition for maintenance of chromatin structure and cell phenotype.

H3.3 dynamics and SAHF formation

Importantly, while formation of SAHF has been associated with the irreversibility of the cell cycle arrest [41,43,73], the molecular basis for their formation has remained elusive [74]. SAHF formation is in part regulated by the H3.3 histone chaperones HIRA and ASF1a [44,47], suggesting involvement of the H3.3 histone variant in this process. Here we show that H3.3 does not localize to SAHF during senescence, but is actually excluded from them **(Fig. 2B and Suppl. Fig. S3C-D)**. Rather, H3.3 is found in transcriptionally active regions in senescent cells, consistent with previous data collected in proliferating cells that showed that H3.3 marks actively transcribed genes [21,22,23,24,25] and is enriched in post-translational modifications associated with the active chromatin state [75,76]. In addition, we did not observe any defects in SAHF formation upon depletion of H3.3 or its chaperones ATRX and DAXX **(Suppl. Fig. S8 and S9)**, suggesting that these proteins are not required for SAHF formation. This is consistent with recent data showing that SAHF are rather formed through the spatial rearrangement of pre-existing heterochromatin [77]. However, absence of H3.3 from SAHF does not preclude its incorporation in other heterochromatic regions such as pericentromeric and telomeric heterochromatin regions **(Fig. 7)**, which localize outside of SAHF [41,42,43,78]. Of note, SAHF are dispensable for cellular senescence and mostly form in response to activated H-Ras in various cell types [79]. Thus, deposition of H3.3, which is not linked to SAHF

formation, might also be an important process for chromatin maintenance in other types of senescence such as replicative senescence, or drug-induced senescence. Interestingly, we observed an enrichment of pre-existing H3.1 at SAHF **(Fig. 1C and 2A-B)**, suggesting that the presence of H3.1 in SAHF may reflect a spatial repositionning of this variant within the H3K9me3-rich core region of SAHF [77], which would be consistent with patterns of repressive post-translational modifications (PTMs) found on H3.1 [75,80].

PML-NBs are novel regulatory sites for H3.3 replication-independent chromatin assembly

While PML-NBs may have specific functions that are crucial for senescence entry [50,51,81], we show that H3.3 is found in PML-NBs in senescent but also in proliferating cells highlighting a novel role for these nuclear bodies as regulatory sites for H3.3 chromatin assembly pathways. We demonstrate that H3.3 localization to PML-NBs is dependent on DAXX, both in proliferating cells (consistent with data obtained in mouse ES cells [26]), and in senescent cells. The structure of DAXX in complex with a dimer of H3.3-H4 [82,83] suggests that H3.3 may be deposited onto PML-NBs as H3.3-H4 dimers. Indeed, a recent study by Delbarre et al. presents experimental evidence for this [84]. In this work, DAXX- dependent H3.3 deposition in PML-NBs was also observed by using transient transfection of epitope-tagged H3.3 in slow growing human cells [84]. Using the SNAP technology, we extend these findings to fast proliferating and senescent cells, indicating that localization to PML-NBs may be a universal replication-independent process of H3.3 targeting to chromatin that operates at all times, maybe also in terminally differentiated cells.

Importantly, while H3.3 is found in complex with the other H3.3 chaperones [26,27,33] **(Fig. 3E)**, its targeting to PML-NBs does not depend on ATRX and HIRA. For ATRX, a possible explanation is that interaction between ATRX and H3.3 may not be direct, but rather be

mediated by DAXX [26]. In addition, recruitment of ATRX to PML-NBs is DAXX-dependent **(Suppl. Fig. S5B and S6)** [60] while the reverse is not true **(Suppl. Fig. S5B)**. Thus, DAXX seems to be the key factor for the recruitment of ATRX and H3.3 to PML-NBs. Interestingly, our analysis performed in senescent cells revealed that ATRX localizes to SAHF in an increased manner when it is no longer targeted to PML-NBs upon DAXX depletion **(Suppl. Fig. S6)**. While localization of ATRX at SAHF may be mediated through an interaction with H3K9me3 and HP1α [85,86], it remains to be determined whether this would have an impact on the chromatin dynamics of the macroH2A variant [87].

Concerning HIRA and its associated chaperone ASF1a, we hypothesize that their localization in PML-NBs together with H3.3 could be a primary event before targeting of H3.3 to active genes [20,27]. Interestingly, PML-NBs associate non-randomly with genomic regions that are transcriptionally active and nascent RNA has been detected in close proximity to PML-NBs [48,62,63,64,88], suggesting that PML-NBs could control transcriptional activities indirectly by participating in the replication-independent assembly of H3.3 **(Fig. 7B-C)**. Of note however, H3.3 loss from PML-NBs upon DAXX depletion does not affect the global incorporation of new H3.3 (**Fig. 4C** and [20]) making it unlikely that localization of H3.3 to PML-NBs is a way to target this histone variant genome-wide. This also potentially explains the absence of a phenotype for the loss of H3.3 from PML-NBs in regards to senescence **(Suppl. Fig. S8 and S9)**. Thus, as suggested in Delbarre et al., PML-NBs may be a gathering point for new H3.3 histones before their targeting to specific genomic locations.

Here we present novel evidence to support this hypothesis. First, we show that large PML-NBs are devoid of transcriptional activity **(Fig. 6C)** and do not contain large amounts of DNA [64], indicating that PML-NBs are unlikely to be direct sites for incorporation of H3.3 into chromatin and may rather represent novel interstages in the replication-independent pathway. Second, we show that upon DAXX overexpression, formation of large PML-NBs is

associated with an accumulation of new H3.3 **(Fig. 5A, Suppl. Fig. S10A)** together with HP1 proteins, independently of H3K9me3 **(Fig. 6D-E)**, consistent with data obtained in ICF cells [89]. These observations strenghten the connection between PML-NBs and heterochromatin components [89,90,91] and support a role of these nuclear bodies in heterochromatin dynamics. We hypothesize that the pool of HP1 could serve for pericentromeric heterochromatin organization together with new H3.3. Whether satellite DNA would directly localize in large PML-NBs as observed in G2 phase in ICF cells [89] is currently not known and should be examined further. Third, we show that depletion of DAXX (which abolishes H3.3 localization in PML-NBs) as well as depletion of PML impairs localization of H3.3 at pericentromeric heterochromatin **(Fig. 7A,C)** and that overexpression of DAXX increases localization of H3.3 at these regions **(Fig. 7D)**, thus implicating PML-NBs in heterochromatin organization. Recent data obtained in mouse ES cells showed that PML depletion impairs chromatin structure at telomeres [92], further underscoring the importance of PML-NBs in heterochromatin maintenance.

Interestingly, failure to organize PML-NBs has been associated with the malignant state of prostate cancer [93], and the ATRX-DAXX-H3.3 pathway is mutated in cancers [34,35,36,37,38,39]. How these chromatin assembly pathways are interconnected remains to be investigated. In summary, our data reveal new elements of chromatin maintenance in proliferating and senescent cells and implicate the enigmatic PML-NBs structures in the replication-independent chromatin assembly pathways.

Materials and Methods

Human cell lines and retroviruses

Human MRC5 primary lung fibroblast (ATCC) and human HEK 293T embryonic kidney cells (Intercell, AG) were cultivated in DMEM medium (GIBCO, Life Technologies). Human IMR90 ER:Ras primary lung fibroblast (a kind gift of Dr. Narita) were cultivated in DMEM medium without phenol red (GIBCO, Life Technologies). 4-hydroxytamoxifen (4-OHT, SIGMA) was added at a concentration of 100nM for 6 days to induce senescence. All media contained 10% FCS (GIBCO, Life Technologies), 100 units/mL of penicillin, 100 µg/mL of streptomycin, and 25 µg/mL of Fungizone® (amphotericin B) (Anti-anti, GIBCO, Life Technologies). MRC5 cell lines stably expressing H3.1-SNAP-HAx3 (e-H3.1), H3.3-SNAP-HAx3 (e-H3.3), Myc-hDAXX or oncogenic Ras (H-RasV12) were established by retroviral transduction [94]. Briefly, pBABE plasmids encoding H3.1-SNAP-HAx3 or H3.3-SNAP-HAx3 (gift from L. Jansen), pLNCX2, pLNCX2 encoding Myc-hDAXX (generated by standart molecular biology procedures), pBABE-puro, pBABE-hygro, pBABE-puro and pBABE-hygro encoding oncogenic Ras [7], pSuper.retro empty or pSuper.retro shDAXX1 [95] or shATRX1 [96] were co-transfected with pCL-ampho plasmid [97] by the calcium phosphate method into HEK 293T cells to package retroviral particles [98]. After 48h, supernatant containing replication-incompetent retroviruses was filtered and applied for 24h on the target MRC5 cells in a medium containing polybrene 8ug/mL (SIGMA) [94]. Stable transfectants were selected with Blasticidin S (5µg/mL, SIGMA), puromycin (1µg/mL, SIGMA), hygromycin (150µg/mL, SIGMA) or neomycin (G418, 1mg/mL, Calbiochem, Millipore) for 3 days and a polyclonal population of cells was used for all experiments. Eventhough levels of expression of H3-SNAP-HAx3 were heterogenous within the cell population, we verified

the global low expression levels of tagged H3.1 and H3.3 by western blot as compared to the endogenous counterparts.

siRNAs, shRNAs and transfections

MRC5 cells were transfected in an antibiotics-free medium for the indicated number of days with 40nM siRNA using Lipofectamine RNAiMax reagent (Invitrogen, Life Technologies) and Opti-MEM 1 medium (GIBCO, Life Technologies) according to manufacturer's instructions. We used the following siRNA sequences: siLuc (non-targeting siRNA against Luciferase): 5'-CGUACGCGGAAUACUUCGA; siDAXX1: 5'-GGAGUUGGAUCUCUCAGAA [99]; siDAXX2: 5'- CAGCCAAGCUCUAUGUCUA [20]; siDAXX3: 5'- CAGAAACAUUAAUAAACAAUA [100]; siATRX1: 5'-GAGGAAACCUUCAAUUGUA [96]; siATRX2: 5'- GCAGAGAAAUUCCUAAAGA [96]; siH3.3A: 5'-CUACAAAAGCCGCUCGCAA [101]; siH3.3B: 5'-GCUAAGAGAGUCACCAUCA [101]; siHIRA: 5'-GGAUAACACUGUCGUCAUC [20]; siPML: 5'- GUGCUUCGAGGCACACCAG [102]. We used siRNAs against H3.3A and H3.3B together, or ATRX1 and ATRX2 together, at a final concentration of 20nM each to achieve depletion of H3.3 and ATRX respectively.

We used the following shRNA sequences cloned into a pSuper.retro vector: shDAXX1: same as siDAXX1 [95], shATRX1: 5'-GATCCCCGAGGAAACCTTCAATTGTATTCAAGAGATACAATTGAAGGTTTCCTCTTTTTA [96].

Antibodies

Supplementary Table SI compiles all primary antibodies used in this study. Company, as well as the order number, the lot number, the species and the dilutions for western blotting (WB) and immunofluorescence (IF) are provided for each antibody.

H3-SNAP Labeling in vivo

The SNAP-labeling protocol is as described in [52,54]. 4μM of SNAP-Block (New England Biolabs) was added during 30 minutes at 37°C to the cell medium to quench the SNAP-tag activity or 2μM of SNAP-Cell TMR-Star (New England Biolabs) during 20 minutes for pulse labeling. After washing of cells with prewarmed PBS, reincubation in complete medium for 30 min allowed excess compound to diffuse from cells and then cells were washed again in PBS. For the chase, incubation of cells was for 3 hours and 30 minutes in complete medium at 37°C. Actinomycin D was added at a dose of 2μg/mL for the total lenght of the chase (3h30) to prevent transcription of new H3.3, or at the end of the chase (for 1h30) to allow synthesis of new H3.3 before transcription inhibition (see **Suppl. Fig. S11**). After *in vivo* labeling, the cells were processed for immunostaining.

Immunofluorescence microscopy

Cells grown on coverslips were directly fixed with 4% formaldehyde or pre-extracted with detergent prior to fixation. Indeed, to detect histones incorporated into chromatin only, soluble proteins were extracted for 2 minutes in cold CSK buffer (10 mM PIPES pH 7, 100 mM NaCl, 300 mM sucrose, 3 mM $MgCl_2$) containing 0.5% of Triton X-100 (SIGMA), and rinsed with CSK and PBS before fixation. For immunofluorescence, we permeabilized cells in PBS containing 0,2% Triton X-100. We then blocked cells with BSA (5% in PBS containing 0.1% Tween 20) for 20 minutes before incubation with primary antibodies **(Suppl. Table SI)** for one hour, followed by washes in PBS 0.1% Tween, and then incubation with secondary

antibodies for 30 minutes. Cross-absorbed Alexa-488, Alexa-594 or Alexa-647 conjugated secondary antibodies (Invitrogen, Molecular probes) were used to detect primary antibodies. Coverslips were mounted in Vectashield (Vector Laboratories) containing DAPI. To label global nascent RNA transcription *in vivo*, we incubated cells with 5-Ethynyl uridine (EU, Invitrogen, Molecular probes), a nucleoside analog of uracil incorporated into RNA during active RNA synthesis, at 1mM for 3 hours. Nascent RNA was revealed with the Click-iT Chemistry (Alexa Fluor 594) according to the manufacturer instructions.

Microscopy Analysis and Quantification of TMR Signal

We acquired images with a DMI600B (Leica) inverted widefield epifluorescence microscope (63X objective/NA 1.32 or 40X objective/NA 1.0) piloted with Leica Application Suite (LAS) and equipped with a Leica DFC365 FX black & white camera or a Leica DFC 295 color camera. We applied identical settings and the same contrast adjustment for all images to allow accurate data comparison, except on Fig. 4C where TMR signal was adjusted to a similar intensity in all conditions to compare localization of new H3.3 at PML-NBs. For brightness and contrast adjustment, we used Adobe Photoshop CS3 (Adobe) and Image J.

To quantify fluorescence intensity (TMR signal) in the acquired images, we used the ImageJ software. Briefly, we defined borders of nuclei using HA immunostaining and we then quantified total gray value for TMR in each nucleus (integrated density). We set a threshold value above which cells were considered as positive for TMR staining and then calculated the number of TMR positive cells for each cell line. We used RGB profiler and interactive 3D surface plot plugins to quantify fluorescence intensity along a line drawn through the nucleus or within all nucleus respectively. A minimum of 100 nuclei was counted in each experiment.

Western blotting

For total extracts, we lysed cells in Laemmli sample buffer (LSB) 1X (62,5mM Tris HCl pH=6.8, 10% glycerol, 2% SDS, 0.002% bromophenol blue and 100mM DTT). For whole cell extracts **(Fig. 1B)**, after two washes in PBS, we lysed cells in lysis buffer (50mM Tris-HCl, pH=7.5, 300mM NaCl, 1mM EDTA, 0.5% NP-40, 5% glycerol) containing protease inhibitors (10µg/mL leupeptin (SIGMA), 10µg/mL of pepstatin A (SIGMA), 100µM PMSF (SIGMA)) and phosphatase inhibitors (5mM sodium fluoride (SIGMA), 10mM β-glycerophosphate (SIGMA), 0.2mM sodium orthovanadate (SIGMA)). We incubated lysates for 20 minutes on ice and then spinned them for 20 minutes at 14 000g. We kept the supernatant as whole cell extracts. For cellular fractionation **(Fig. 3E, Suppl. Fig. S3B)**, we performed cytosolic and nuclear extracts as described in [80,103] with buffers containing protease and phosphatase inhibitors as described above. We loaded extracts on SDS-polyacrylamide gels and performed electrophoresis. We used Ponceau 1% (SIGMA) to detect proteins transferred on nitrocellulose membranes. We used primary antibodies as described in **Suppl. Table SI**. We used secondary antibodies conjugated with Horseradish peroxidase (HRP) (GE Healthcare Life sciences) and revealed signal by chemiluminescence substrate from Amerscham (SuperSignal West Pico or SuperSignal West Femto) (GE Healthcare Life sciences).

Immunoprecipitation

For immunoprecipitation, we used 150µg of Nuclear extracts from plain MRC5, or MRC5 e-H3.1 and MRC5 e-H3.3 transduced with pBABE-puro or pBABE-puro-H-RasV12 retroviruses for 8 days. We performed the immunoprecipitation for 2 hours with HA beads (SIGMA A2095 clone HA-7) in IP buffer (20 mM Tris at pH 7.6, 150 mM NaCl, 3 mM MgCl2, 0.1 mM EDTA, 10% glycerol, 0.1% NP-40) containing protease and phosphatase inhibitors as described above. After 3 washes in IP buffer with a 5 minutes incubation at 4°C

for each wash, beads were resuspended in LSB 1X buffer and 100mM DTT, boiled 10 minutes and the supernatant was then loaded on an SDS-polyacrylamide gel for further Western Blot analysis.

Chromatin immunoprecipitation (ChIP)

ChiP was performed as described in [104]. Briefly, MRC5, MRC5 e-H3.1 or e-H3.3 cells, treated or not with siRNAs for 72 hours, or transduced with viruses encoding Myc-DAXX for overexpression of DAXX for 7 days, were crosslinked in 1% formaldehyde for 10 minutes at room temperature. After stopping the reaction with 0.125M of Glycine for 5 minutes at room temperature, cells were washed in PBS, scraped in a tube and lysed in 85mM KCl, 5mM PIPES pH=8.0, 1% NP-40 containing leupeptin (10mg/mL), pepstatin (10mg/mL) and PMSF (1mM) for 15 minutes on ice. Cells were homogenized using a glass dounce homogenizer and nuclei were released with 20 strokes on ice. After centrifugation, nuclei were subsequently lysed in nuclei lysis buffer containing 50 mM Tris–HCl pH=8.0, 10 mM EDTA, 1% SDS and protease inhibitors as described above. Sonication was performed using a Bioruptor (Diagenode) for 30 minutes with 30s ON-30s OFF pulses to achieve an average chromatin length of 200–500 bp. After centrifugation, chromatin from 4x10e6 cells was diluted 5 times in ChIP dilution buffer (50 mM Tris–HCl pH=7.4,150 mM NaCl, 1% NP-40, 0.25% sodium deoxycholic acid, 1mM EDTA pH=8.0 containing protease inhibitors as described above) and immunoprecipitated overnight at 4°C with 1μg of Rabbit IgG or HA antibody. Protein A agarose beads (Millipore #16-157) were added for 2 hours at 4°C. After extensive washes as described in [104], bound chromatin was eluted for 30 minutes in elution buffer (50mM NaHCO3, 1% SDS) and decrosslinked overnight at 67°C in the elution buffer containing 0.54M NaCl. Samples from input chromatin (10%) were diluted 4 times in elution buffer containing 0.54M NaCl and decrosslinked as ChIP samples. After treatment of samples with

RNaseA for 20 minutes at 37°C, DNA was purified with PCR purification kit (QIAGEN). Quantitative PCR was performed as described in Supplementary Materials and methods.

Acknowledgments

We thank all members of the departement of gynecology for help and discussion, and especially Dorthe Larsen for fruitful discussions, Geneviève Almouzni for valuable advice and for rabbit ASF1a and PML antibodies, Lars Jansen for the pBABE-H3.1-SNAP-HAx3 and pBABE-H3.3-SNAP-HAx3 plasmids, Fabrizio d'Adda di Fagagna for the pBABE-puro/hygro and pBABE-puro-/hygro-H-RasV12 plasmids, Nathalie Berube for the pSuper.retro.neo shATRX1 and shATRX2, Wade Bresnahan for the pSuper.retro.puro shDAXX and Masashi Narita for providing the IMR90 ER:Ras cells. Confocal imaging was performed with support from the Center for Microscopy and Image Analysis, University of Zurich. This work was supported by grants from the Swiss National Foundation (project grant 31003A-127450 to M.S. and Marie-Heim Vögtlin grant PMPDP3_139706 to A.C.) and by the Kanton of Zürich.

Author contributions

A.C. and M.S. designed research. A.C., T.O., M.G. performed research. D.F. contributed to research. A.C. analyzed data. A.C. and M.S. wrote the paper.

The authors declare that they have no conflict of interest**.**

References

1. Hayflick L, Moorhead PS. The serial cultivation of human diploid cell strains. Experimental Cell Research 1961; 25:585–621.

2. Adams PD. Remodeling of chromatin structure in senescent cells and its potential impact on tumor suppression and aging. Gene 2007; 397:84–93.

3. Narita M. Cellular senescence and chromatin organisation. Br J Cancer 2007; 96:686–691.

4. Serrano M, Lin AW, McCurrach ME, Beach D, Lowe SW. Oncogenic ras provokes premature cell senescence associated with accumulation of p53 and p16INK4a. Cell 1997; 88:593–602.

5. Ramirez RD. Putative telomere-independent mechanisms of replicative aging reflect inadequate growth conditions. Genes & Development 2001; 15:398–403.

6. Bartkova J, Rezaei N, Liontos M, Karakaidos P, Kletsas D, Issaeva N, Vassiliou L-VF, Kolettas E, Niforou K, Zoumpourlis VC, Takaoka M, Nakagawa H, Tort F, Fugger K, Johansson F, Sehested M, Andersen CL, Dyrskjot L, Ørntoft T, Lukas J, Kittas C, Helleday T, Halazonetis TD, Bartek J, Gorgoulis VG. Oncogene-induced senescence is part of the tumorigenesis barrier imposed by DNA damage checkpoints [Internet]. Nature 2006; 444:633–637.

7. Di Micco R, Fumagalli M, Cicalese A, Piccinin S, Gasparini P, Luise C, Schurra C, Garre M, Giovanni Nuciforo P, Bensimon A, Maestro R, Giuseppe Pelicci P, D'adda Di Fagagna F. Oncogene-induced senescence is a DNA damage response triggered by DNA hyper-replication. Nature 2006; 444:638–642.

8. Mallette FA, Gaumont-Leclerc M-F, Ferbeyre G. The DNA damage signaling pathway is a critical mediator of oncogene-induced senescence. Genes & Development 2007; 21:43–48.

9. Michaloglou C, Vredeveld LCW, Soengas MS, Denoyelle C, Kuilman T, van der Horst CMAM, Majoor DM, Shay JW, Mooi WJ, Peeper DS. BRAFE600-associated senescence-like cell cycle arrest of human naevi. Nat Cell Biol 2005; 436:720–724.

10. Collado M, Gil J, Efeyan A, Guerra C, Schuhmacher AJ, Barradas M, Benguría A, Zaballos A, Flores JM, Barbacid M, Beach D, Serrano M. Tumour biology: Senescence in premalignant tumours. Nat Cell Biol 2005; 436:642–642.

11. Chen Z, Trotman LC, Shaffer D, Lin H-K, Dotan ZA, Niki M, Koutcher JA, Scher HI, Ludwig T, Gerald W, Cordon-Cardo C, Paolo Pandolfi P. Crucial role of p53-dependent cellular senescence in suppression of Pten-deficient tumorigenesis. Nat Cell Biol 2005; 436:725–730.

12. Denchi EL, Attwooll C, Pasini D, Helin K. Deregulated E2F Activity Induces Hyperplasia and Senescence-Like Features in the Mouse Pituitary Gland. Molecular and Cellular Biology 2005; 25:2660–2672.

13. Braig M, Lee S, Loddenkemper C, Rudolph C, Peters AHFM, Schlegelberger B, Stein H, Dörken B, Jenuwein T, Schmitt CA. Oncogene-induced senescence as an initial barrier in lymphoma development. Nat Cell Biol 2005; 436:660–665.

14. Luger K, Dechassa ML, Tremethick DJ. New insights into nucleosome and chromatin structure: an ordered state or a disordered affair? Nature Reviews Molecular Cell Biology 2012; 13:436–447.

15. Burgess RJ, Zhang Z. Histone chaperones in nucleosome assembly and human disease. Nat Struct Mol Biol 2013; 20:14–22.

16. Talbert PB, Henikoff S. Histone variants — ancient wrap artists of the epigenome. Nature Reviews Molecular Cell Biology 2010; 11:264–275.

17. Szenker E, Ray-Gallet D, Almouzni G. The double face of the histone variant H3.3. Cell Res 2011; 1–14.

18. Wu RS, Tsai S, Bonner WM. Patterns of histone variant synthesis can distinguish G0 from G1 cells. Cell 1982; 31:367–374.

19. Tagami H, Ray-Gallet D, Almouzni G, Nakatani Y. Histone H3.1 and H3.3 complexes mediate nucleosome assembly pathways dependent or independent of DNA synthesis. Cell 2004; 116:51–61.

20. Ray-Gallet D, Woolfe A, Vassias I, Pellentz C, Lacoste N, Puri A, Schultz DC, Pchelintsev NA, Adams PD, Jansen LET, Almouzni G. Dynamics of Histone H3 Deposition In Vivo Reveal a Nucleosome Gap-Filling Mechanism for H3.3 to Maintain Chromatin Integrity. Molecular Cell 2011; 44:928–941.

21. Ahmad K and Henikoff S. The Histone variant H3.3 marks active chromatin by replication-independent nucleosome assembly. Molecular Cell 2002; 9:1191–1200.

22. Mito Y, Henikoff JG, Henikoff S. Genome-scale profiling of histone H3.3 replacement patterns. Nat Genet 2005; 37:1090–1097.

23. Wirbelauer C. Variant histone H3.3 is deposited at sites of nucleosomal displacement throughout transcribed genes while active histone modifications show a promoter-proximal bias. Genes & Development 2005; 19:1761–1766.

24. Jin C, Zang C, Wei G, Cui K, Peng W, Zhao K, Felsenfeld G. H3.3/H2A.Z double variant-containing nucleosomes mark “nucleosome-free regions” of active promoters and other regulatory regions. Nat Genet 2009; 41:941–945.

25. Chow C-M, Georgiou A, Szutorisz H, Maia E Silva A, Pombo A, Barahona I, Dargelos E, Canzonetta C, Dillon N. Variant histone H3.3 marks promoters of transcriptionally active genes during mammalian cell division. EMBO Rep 2005;

6:354–360.

26. Drane P, Ouararhni K, Depaux A, Shuaib M, Hamiche A. The death-associated protein DAXX is a novel histone chaperone involved in the replication-independent deposition of H3.3. Genes & Development 2010; 24:1253–1265.

27. Goldberg AD, Banaszynski LA, Noh K-M, Lewis PW, Elsaesser SJ, Stadler S, Dewell S, Law M, Guo X, Li X, Wen D, Chapgier A, Dekelver RC, Miller JC, Lee Y-L, Boydston EA, Holmes MC, Gregory PD, Greally JM, Rafii S, Yang C, Scambler PJ, Garrick D, Gibbons RJ, Higgs DR, Cristea IM, Urnov FD, Zheng D, Allis CD. Distinct factors control histone variant H3.3 localization at specific genomic regions. Cell 2010; 140:678–691.

28. Wong LH, Ren H, Williams E, McGhie J, Ahn S, Sim M, Tam A, Earle E, Anderson MA, Mann J, Choo KHA. Histone H3.3 incorporation provides a unique and functionally essential telomeric chromatin in embryonic stem cells. Genome Research 2008; 19:404–414.

29. Ray-Gallet D, Quivy J-P, Scamps C, Martini EM-D, Lipinski M, Almouzni G. HIRA is critical for a nucleosome assembly pathway independent of DNA synthesis. Molecular Cell 2002; 9:1091–1100.

30. Balaji S, Iyer LM, Aravind L. HPC2 and ubinuclein define a novel family of histone chaperones conserved throughout eukaryotes. Mol. BioSyst. 2009; 5:269.

31. Banumathy G, Somaiah N, Zhang R, Tang Y, Hoffmann J, Andrake M, Ceulemans H, Schultz D, Marmorstein R, Adams PD. Human UBN1 Is an Ortholog of Yeast Hpc2p and Has an Essential Role in the HIRA/ASF1a Chromatin-Remodeling Pathway in Senescent Cells. Molecular and Cellular Biology 2009; 29:758–770.

32. Rai TS, Puri A, McBryan T, Hoffman J, Tang Y, Pchelintsev NA, van Tuyn J, Marmorstein R, Schultz DC, Adams PD. Human CABIN1 Is a Functional Member of the Human HIRA/UBN1/ASF1a Histone H3.3 Chaperone Complex. Molecular and Cellular Biology 2011; 31:4107–4118.

33. Lewis PW, Elsaesser SJ, Noh K-M, Stadler SC, Allis CD. Daxx is an H3.3-specific histone chaperone and cooperates with ATRX in replication-independent chromatin assembly at telomeres. Proceedings of the National Academy of Sciences 2010; 107:14075–14080.

34. Schwartzentruber J, Korshunov A, Liu X-Y, Jones DTW, Pfaff E, Jacob K, Sturm D, Fontebasso AM, Quang D-AK, Tönjes M, Hovestadt V, Albrecht S, Kool M, Nantel A, Konermann C, Lindroth A, Jäger N, Rausch T, Ryzhova M, Korbel JO, Hielscher T, Hauser P, Garami M, Klekner A, Bognar L, Ebinger M, Schuhmann MU, Scheurlen W, Pekrun A, Frühwald MC, Roggendorf W, Kramm C, Dürken M, Atkinson J, Lepage P, Montpetit A, Zakrzewska M, Zakrzewski K, Liberski PP, Dong Z, Siegel P, Kulozik AE, Zapatka M, Guha A, Malkin D, Felsberg J, Reifenberger G, Deimling von A, Ichimura K, Collins VP, Witt H, Milde T, Witt O, Zhang C, Castelo-Branco P, Lichter P, Faury D, Tabori U, Plass C, Majewski J, Pfister SM, Jabado N. Driver mutations in histone H3.3 and chromatin remodelling genes in paediatric glioblastoma. Nature 2012; 1–7.

35. Wu, Gang Wu, Alberto Broniscer, Troy A McEachron, Lu C, Paugh BS, Becksfort J, Qu C, Ding L, Huether R, Parker M, Zhang J, Gajjar A, Dyer MA, Mullighan CG, Gilbertson RJ, Mardis ER, Wilson RK, Downing JR, Ellison DW, Baker JZSJ. Somatic histone H3 alterations in pediatric diffuse intrinsic pontine gliomas and non-brainstem glioblastomas [Internet]. Nature Publishing Group 2012; 1–3.

36. Sturm D, Witt H, Hovestadt V, Khuong-Quang D-A, Jones DTW, Konermann C, Pfaff E, Tönjes M, Sill M, Bender S, Kool M, Zapatka M, Becker N, Zucknick M, Hielscher T, Liu X-Y, Fontebasso AM, Ryzhova M, Albrecht S, Jacob K, Wolter M, Ebinger M, Schuhmann MU, van Meter T, Frühwald MC, Hauch H, Pekrun A, Radlwimmer B, Niehues T, Komorowski von G, Dürken M, Kulozik AE, Madden J, Donson A, Foreman NK, Drissi R, Fouladi M, Scheurlen W, Deimling von A, Monoranu C, Roggendorf W, Herold-Mende C, Unterberg A, Kramm CM, Felsberg J, Hartmann C, Wiestler B, Wick W, Milde T, Witt O, Lindroth AM, Schwartzentruber J, Faury D, Fleming A, Zakrzewska M, Liberski PP, Zakrzewski K, Hauser P, Garami M, Klekner A, Bognar L, Morrissy S, Cavalli F, Taylor MD, van Sluis P, Koster J, Versteeg R, Volckmann R, Mikkelsen T, Aldape K, Reifenberger G, Collins VP, Majewski J, Korshunov A, Lichter P, Plass C, Jabado N, Pfister SM. Hotspot Mutations in H3F3A and IDH1 Define Distinct Epigenetic and Biological Subgroups of Glioblastoma. Cancer Cell 2012; 22:425–437.

37. Khuong-Quang D-A, Buczkowicz P, Rakopoulos P, Liu X-Y, Fontebasso AM, Bouffet E, Bartels U, Albrecht S, Schwartzentruber J, Letourneau L, Bourgey M, Bourque G, Montpetit A, Bourret G, Lepage P, Fleming A, Lichter P, Kool M, Deimling A, Sturm D, Korshunov A, Faury D, Jones DT, Majewski J, Pfister SM, Jabado N, Hawkins C. K27M mutation in histone H3.3 defines clinically and biologically distinct subgroups of pediatric diffuse intrinsic pontine gliomas. Acta Neuropathol 2012; 124:439–447.

38. Jiao Y, Shi C, Edil BH, de Wilde RF, Klimstra DS, Maitra A, Schulick RD, Tang LH, Wolfgang CL, Choti MA, Velculescu VE, Diaz LA, Vogelstein B, Kinzler KW, Hruban RH, Papadopoulos N. DAXX/ATRX, MEN1, and mTOR pathway genes are frequently altered in pancreatic neuroendocrine tumors. Science 2011; 331:1199–1203.

39. Heaphy CM, de Wilde RF, Jiao Y, Klein AP, Edil BH, Shi C, Bettegowda C, Rodriguez FJ, Eberhart CG, Hebbar S, Offerhaus GJ, McLendon R, Rasheed BA, He Y, Yan H, Bigner DD, Oba-Shinjo SM, Marie SKN, Riggins GJ, Kinzler KW, Vogelstein B, Hruban RH, Maitra A, Papadopoulos N, Meeker AK. Altered telomeres in tumors with ATRX and DAXX mutations. Science 2011; 333:425.

40. Papamichos-Chronakis M, Peterson CL. Chromatin and the genome integrity network. Nature Reviews Genetics 2013; 14:62–75.

41. Narita M, Nũnez S, Heard E, Narita M, Lin AW, Hearn SA, Spector DL, Hannon GJ, Lowe SW. Rb-mediated heterochromatin formation and silencing of E2F target genes during cellular senescence. Cell 2003; 113:703–716.

42. Di Micco R, Sulli G, Dobreva M, Liontos M, Botrugno OA, Gargiulo G, Dal Zuffo R,

Matti V, D'ario G, Montani E, Mercurio C, Hahn WC, Gorgoulis V, Minucci S, d'Adda di Fagagna F. Interplay between oncogene-induced DNA damage response and heterochromatin in senescence and cancer. Nat Cell Biol 2011; 13:292–302.

43. Narita M, Narita M, Krizhanovsky V, Nuñez S, Chicas A, Hearn SA, Myers MP, Lowe SW. A novel role for high-mobility group a proteins in cellular senescence and heterochromatin formation. Cell 2006; 126:503–514.

44. Zhang R, Poustovoitov MV, Ye X, Santos HA, Chen W, Daganzo SM, Erzberger JP, Serebriiskii IG, Canutescu AA, Dunbrack RL. Formation of MacroH2A-Containing Senescence-Associated Heterochromatin Foci and Senescence Driven by ASF1a and HIRA. Developmental Cell 2005; 8:19–30.

45. Costanzi C, Pehrson JR. Histone macroH2A1 is concentrated in the inactive X chromosome of female mammals. Nature 1998; 393:599–601.

46. Rai TS, Adams PD. Lessons from senescence: Chromatin maintenance in non-proliferating cells. BBA - Gene Regulatory Mechanisms 2011; 1–10.

47. Ye X, Zerlanko B, Zhang R, Somaiah N, Lipinski M, Salomoni P, Adams PD. Definition of pRB- and p53-Dependent and -Independent Steps in HIRA/ASF1a-Mediated Formation of Senescence-Associated Heterochromatin Foci. Molecular and Cellular Biology 2007; 27:2452–2465.

48. Bernardi R, Pandolfi PP. Structure, dynamics and functions of promyelocytic leukaemia nuclear bodies. Nature Reviews Molecular Cell Biology 2007; 8:1006–1016.

49. Lallemand-Breitenbach V, de The H. PML Nuclear Bodies. Cold Spring Harbor Perspectives in Biology 2010; 2:a000661–a000661.

50. Pearson M, Carbone R, Sebastiani C, Cioce M, Fagioli M, Saito S, Higashimoto Y, Appella E, Minucci S, Pandolfi PP, Pelicci PG. PML regulates p53 acetylation and premature senescence induced by oncogenic Ras. Nature 2000; 406:207–210.

51. Ferbeyre G, de Stanchina E, Querido E, Baptiste N, Prives C, Lowe SW. PML is induced by oncogenic ras and promotes premature senescence. Genes & Development 2000; 14:2015–2027.

52. Jansen LET, Black BE, Foltz DR, Cleveland DW. Propagation of centromeric chromatin requires exit from mitosis. J Cell Biol 2007; 176:795–805.

53. Keppler A, Gendreizig S, Gronemeyer T, Pick H, Vogel H, Johnsson K. A general method for the covalent labeling of fusion proteins with small molecules in vivo. Nat Biotechnol 2002; 21:86–89.

54. Bodor DL, Rodríguez MG, Moreno N, Jansen LET. Analysis of protein turnover by quantitative SNAP-based pulse-chase imaging. Curr Protoc Cell Biol 2012; Chapter 8:Unit8.8.

55. Dimri GP, Lee X, Basile G, Acosta M, Scott G, Roskelley C, Medrano EE, Linskens M, Rubelj I, Pereira-Smith O. A biomarker that identifies senescent human cells in culture and in aging skin in vivo. Proc Natl Acad Sci USA 1995; 92:9363–9367.

56. Debacq-Chainiaux F, Erusalimsky JD, Campisi J, Toussaint O. Protocols to detect senescence-associated beta-galactosidase (SA-βgal) activity, a biomarker of senescent cells in culture and in vivo. Nature Protocols 2009; 4:1798–1806.

57. Young ARJ, Narita M, Ferreira M, Kirschner K, Sadaie M, Darot JFJ, Tavare S, Arakawa S, Shimizu S, Watt FM, Narita M. Autophagy mediates the mitotic senescence transition. Genes & Development 2009; 23:798–803.

58. Corpet A, De Koning L, Toedling J, Savignoni A, Berger F, Lemaître C, O'Sullivan RJ, Karlseder J, Barillot E, Asselain B, Sastre-Garau X, Almouzni G. Asf1b, the necessary Asf1 isoform for proliferation, is predictive of outcome in breast cancer. The EMBO Journal 2010; 30:480–493.

59. Xue Y, Gibbons R, Yan Z, Yang D, McDowell TL, Sechi S, Qin J, Zhou S, Higgs D, Wang W. The ATRX syndrome protein forms a chromatin-remodeling complex with Daxx and localizes in promyelocytic leukemia nuclear bodies. Proc Natl Acad Sci USA 2003; 100:10635–10640.

60. Ishov AM. Heterochromatin and ND10 are cell-cycle regulated and phosphorylation-dependent alternate nuclear sites of the transcription repressor Daxx and SWI/SNF protein ATRX. Journal of Cell Science 2004; 117:3807–3820.

61. Jiang W-Q, Nguyen A, Cao Y, Chang AC-M, Reddel RR. HP1-Mediated Formation of Alternative Lengthening of Telomeres-Associated PML Bodies Requires HIRA but Not ASF1a. PLoS ONE 2011; 6:e17036.

62. Wang J. Promyelocytic leukemia nuclear bodies associate with transcriptionally active genomic regions. J Cell Biol 2004; 164:515–526.

63. Kiesslich A, Mikecz von A, Hemmerich P. Cell cycle-dependent association of PML bodies with sites of active transcription in nuclei of mammalian cells. J. Struct. Biol. 2002; 140:167–179.

64. Boisvert F-M, Hendzel MJ, Bazett-Jones DP. Promyelocytic leukemia (PML) nuclear bodies are protein structures that do not accumulate RNA. J Cell Biol 2000; 148:283–292.

65. Maison C, Almouzni G. HP1 and the dynamics of heterochromatin maintenance. Nature Publishing Group 2004; 5:296–305.

66. Morozov VM, Gavrilova EV, Ogryzko VV, Ishov AM. Dualistic function of Daxx at centromeric and pericentromeric heterochromatin in normal and stress conditions. nucleus 2012; 3:

67. Deal RB, Henikoff JG, Henikoff S. Genome-Wide Kinetics of Nucleosome

Turnover Determined by Metabolic Labeling of Histones. Science 2010; 328:1161–1164.

68. De Cecco M, Jeyapalan J, Zhao X, Tamamori-Adachi M, Sedivy JM. Nuclear protein accumulation in cellular senescence and organismal aging revealed with a novel single-cell resolution fluorescence microscopy assay. Aging (Albany NY) 2011; 3:955–967.

69. Lopez MF, Tollervey J, Krastins B, Garces A, Sarracino D, Prakash A, Vogelsang M, Geesman G, Valderrama A, Jordan IK, Lunyak VV. Depletion of nuclear histone H2A variants is associated with chronic DNA damage signaling upon drug-evoked senescence of human somatic cells. Aging (Albany NY) 2012; 4:823–842.

70. O'Sullivan RJ, Kubicek S, Schreiber SL, Karlseder J. Reduced histone biosynthesis and chromatin changes arising from a damage signal at telomeres. Nat Struct Mol Biol 2010; 17:1218–1225.

71. Polo SE, Theocharis SE, Klijanienko J, Savignoni A, Asselain B, Vielh P, Almouzni G. Chromatin assembly factor-1, a marker of clinical value to distinguish quiescent from proliferating cells. Cancer Research 2004; 64:2371–2381.

72. Ng RK, Gurdon JB. Epigenetic memory of an active gene state depends on histone H3.3 incorporation into chromatin in the absence of transcription. Nat Cell Biol 2007; 10:102–109.

73. Beauséjour CM, Krtolica A, Galimi F, Narita M, Lowe SW, Yaswen P, Campisi J. Reversal of human cellular senescence: roles of the p53 and p16 pathways [Internet]. The EMBO Journal 2003; 22:4212–4222.

74. Chandra T, Narita M. High-order chromatin structure and the epigenome in SAHFs. nucleus 2013; 4:23–28.

75. Hake SB, Garcia BA, Duncan EM, Kauer M, Dellaire G, Shabanowitz J, Bazett-Jones DP, Allis CD, Hunt DF. Expression patterns and post-translational modifications associated with mammalian histone H3 variants. J Biol Chem 2006; 281:559–568.

76. McKittrick E, Gafken PR, Ahmad K, Henikoff S. Histone H3.3 is enriched in covalent modifications associated with active chromatin. Proc Natl Acad Sci USA 2004; 101:1525–1530.

77. Chandra T, Kirschner K, Thuret J-Y, Pope BD, Ryba T, Newman S, Ahmed K, Samarajiwa SA, Salama R, Carroll T, Stark R, Janky R, Narita M, Xue L, Chicas A, Nũnez S, Janknecht R, Hayashi-Takanaka Y, Wilson MD, Marshall A, Odom DT, Babu MM, Bazett-Jones DP, Tavaré S, Edwards PAW, Lowe SW, Kimura H, Gilbert DM, Narita M. Independence of Repressive Histone Marks and Chromatin Compaction during Senescent Heterochromatic Layer Formation. Molecular Cell 2012; 47:203–214.

78. Zhang R, Chen W, Adams PD. Molecular Dissection of Formation of

Senescence-Associated Heterochromatin Foci. Molecular and Cellular Biology 2007; 27:2343–2358.

79. Kosar M, Bartkova J, Hubackova S, Hodny Z, Lukas J, Bartek J. Senescence-associated heterochromatin foci are dispensable for cellular senescence, occur in a cell type- and insult-dependent manner and follow expression of p16 ink4a. Cell Cycle 2011; 10:457–468.

80. Loyola A, Bonaldi T, Roche D, Imhof A, Almouzni G. PTMs on H3 Variants before Chromatin Assembly Potentiate Their Final Epigenetic State. Molecular Cell 2006; 24:309–316.

81. de Stanchina E, Querido E, Narita M, Davuluri RV, Pandolfi PP, Ferbeyre G, Lowe SW. PML is a direct p53 target that modulates p53 effector functions. Molecular Cell 2004; 13:523–535.

82. Elsässer SJ, Huang H, Lewis PW, Chin JW, Allis CD, Patel DJ. DAXX envelops an H3.3-H4 dimer for H3.3-specific recognition. Nature 2012; 1–8.

83. Liu C-P, Xiong C, Wang M, Yu Z, Yang N, Chen P, Zhang Z, Li G, Xu R-M. Structure of the variant histone H3.3–H4 heterodimer in complex with its chaperone DAXX. Nat Struct Mol Biol 2012; 19:1287–1292.

84. Delbarre E, Ivanauskiene K, Küntziger T, Collas P. DAXX-dependent supply of soluble (H3.3-H4) dimers to PML bodies pending deposition into chromatin. Genome Research 2013;

85. Dhayalan A, Tamas R, Bock I, Tattermusch A, Dimitrova E, Kudithipudi S, Ragozin S, Jeltsch A. The ATRX-ADD domain binds to H3 tail peptides and reads the combined methylation state of K4 and K9. Human Molecular Genetics 2011; 20:2195–2203.

86. Lechner MS, Schultz DC, Negorev D, Maul GG, Rauscher FJ III. The mammalian heterochromatin protein 1 binds diverse nuclear proteins through a common motif that targets the chromoshadow domain. Biochemical and Biophysical Research Communications 2005; 331:929–937.

87. Ratnakumar K, Duarte LF, LeRoy G, Hasson D, Smeets D, Vardabasso C, Bonisch C, Zeng T, Xiang B, Zhang DY, Li H, Wang X, Hake SB, Schermelleh L, Garcia BA, Bernstein E. ATRX-mediated chromatin association of histone variant macroH2A1 regulates -globin expression. Genes & Development 2012; 26:433–438.

88. Dellaire G, Bazett-Jones DP. PML nuclear bodies: dynamic sensors of DNA damage and cellular stress. Bioessays 2004; 26:963–977.

89. Luciani JJ. PML nuclear bodies are highly organised DNA-protein structures with a function in heterochromatin remodelling at the G2 phase. Journal of Cell Science 2006; 119:2518–2531.

90. Seeler JS, Marchio A, Sitterlin D, Transy C, Dejean A. Interaction of SP100 with

HP1 proteins: a link between the promyelocytic leukemia-associated nuclear bodies and the chromatin compartment. Proc Natl Acad Sci USA 1998; 95:7316–7321.

91. Kepkay R, Attwood KM, Ziv Y, Shiloh Y, Dellaire G. KAP1 depletion increases PML nuclear body number in concert with ultrastructural changes in chromatin. Cell Cycle 2011; 10:308–322.

92. Chang FTM, McGhie JD, Chan FL, Tang MC, Anderson MA, Mann JR, Andy Choo KH, Wong LH. PML bodies provide an important platform for the maintenance of telomeric chromatin integrity in embryonic stem cells. Nucleic Acids Research 2013; 41:4447–4458.

93. Vernier M, Bourdeau V, Gaumont-Leclerc M-F, Moiseeva O, Begin V, Saad F, Mes-Masson A-M, Ferbeyre G. Regulation of E2Fs and senescence by PML nuclear bodies. Genes & Development 2011; 25:41–50.

94. Pear W. Transient transfection methods for preparation of high-titer retroviral supernatants. Curr Protoc Mol Biol 2001; Chapter 9:Unit9.11.

95. Cantrell SR, Bresnahan WA. Human Cytomegalovirus (HCMV) UL82 Gene Product (pp71) Relieves hDaxx-Mediated Repression of HCMV Replication. Journal of Virology 2006; 80:6188–6191.

96. Ritchie K, Seah C, Moulin J, Isaac C, Dick F, Berube NG. Loss of ATRX leads to chromosome cohesion and congression defects. J Cell Biol 2008; 180:315–324.

97. Naviaux RK, Costanzi E, Haas M, Verma IM. The pCL vector system: rapid production of helper-free, high-titer, recombinant retroviruses. Journal of Virology 1996; 70:5701–5705.

98. Sambrook J, Russell DW. Calcium-phosphate-mediated Transfection of Eukaryotic Cells with Plasmid DNAs. CSH Protoc 2006; 2006:

99. Chen LY, Chen JD. Daxx Silencing Sensitizes Cells to Multiple Apoptotic Pathways. Molecular and Cellular Biology 2003; 23:7108–7121.

100. Zhang X, Gu L, Li J, Shah N, He J, Yang L, Hu Q, Zhou M. Degradation of MDM2 by the Interaction between Berberine and DAXX Leads to Potent Apoptosis in MDM2-Overexpressing Cancer Cells. Cancer Research 2010; 70:9895–9904.

101. Zhang R, Liu S-T, Chen W, Bonner M, Pehrson J, Yen TJ, Adams PD. HP1 Proteins Are Essential for a Dynamic Nuclear Response That Rescues the Function of Perturbed Heterochromatin in Primary Human Cells. Molecular and Cellular Biology 2007; 27:949–962.

102. Perfettini J-L, Nardacci R, Séror C, Bourouba M, Subra F, Gros L, Manic G, Amendola A, Masdehors P, Rosselli F, Ojcius DM, Auclair C, de The H, Gougeon M-L, Piacentini M, Kroemer G. The tumor suppressor protein PML controls apoptosis induced by the HIV-1 envelope. Cell Death and Differentiation 2008; 16:298–311.

103. Martini E, Roche DM, Marheineke K, Verreault A, Almouzni G. Recruitment of phosphorylated chromatin assembly factor 1 to chromatin after UV irradiation of human cells. J Cell Biol 1998; 143:563–575.

104. O'Geen H, Echipare L, Farnham PJ. Using ChIP-Seq Technology to Generate High-Resolution Profiles of Histone Modifications. In: Methods in Molecular Biology. Totowa, NJ: Humana Press; 2011. :265–286.

Figure legends

Figure 1: Dynamics of H3.1 and H3.3 deposition in proliferating and senescent human cells.

A. Fluorescent microscopy visualization of H3.1- and H3.3-SNAP-HAx3 after *in vivo* labeling assays of MRC5 human primary cells with red fluorescent TMR-Star in pulse, quench-pulse, and quench-chase-pulse experiments. The pulse labels pre-existing H3-SNAP, the quench-pulse quenches pre-existing H3-SNAP with nonfluorescent block preventing their subsequent labeling with TMR-Star (background), and the quench-chase-pulse labels new H3-SNAP synthesized during the 3h30 chase. In all cases, HA stains total histone H3. DAPI stains nuclei. Scale bar is 10 μm. (See also **Suppl. Fig. S1**).

B. Western blot analysis of whole cell extracts from MRC5 stably expressing H3.1- or H3.3 SNAP-HAx3 (e-H3.1 and e-H3.3, respectively) and transduced with an empty retroviral vector (empty) or with a vector expressing H-RasV12 (Ras) for 10 days. 25μg of protein extracts were loaded. HA and Ras stainings verified expression of the transduced proteins. Mcm7 was used as a marker for cell proliferation and p16 as a marker for proliferation arrest. Smc-1 served as a loading control. M: molecular weight marker. (See also **Suppl. Fig. S2A-C**).

C. Fluorescent microscopy visualization of new H3.1 and H3.3 (TMR, red) after *in vivo* labelling of MRC5 e-H3.1 and e-H3.3 treated as in (B) in a quench-chase-pulse experiment. HA (green) stains total H3 histones and DAPI stains nuclei. Scale bar is 10 μm. (See also **Suppl. Fig. S2D**).

D. Histogram shows quantitative analysis of the proportion of TMR positive cells in MRC5 e-H3.1 or e-H3.3 proliferating (empty) and senescent (Ras) cells. Numbers represent the mean of 3 independent experiments ± s.d.

Figure 2: New H3.3 deposition does not occur into SAHF, in contrast to parental H3.1, but correlates with transcriptional activity in human senescent cells.

A. Fluorescent microscopy visualization of pre-existing H3.1 (HA, green) in MRC5 e-H3.1 cells proliferating (empty) or induced into senescence with H-RasV12 overexpression (Ras) for 8 days. H3K9me3 (red) and DAPI were used as markers for SAHF formation. Scale bar is 10 μm.

B. Graphics show fluorescent intensity profiles quantified by Image J along lines drawn through nuclei as shown in panel (A).

C. Fluorescent microscopy visualization of nascent global RNA transcription *in vivo* in MRC5 cells treated as in (A). Nascent RNAs were labeled with 5-ethynyl uridine (EU) for 3 hours and revealed by the Click-iT chemistry (red). H3K9me3 (green) and DAPI were used as markers for SAHF formation. Scale bar is 10 μm.

D. Graphics show fluorescent intensity profiles quantified using Image J along lines drawn through nuclei as shown in panel (C).

E. Fluorescent microscopy visualization of new H3.3 (TMR, red) after *in vivo* labelling of MRC5 e-H3.3 cells treated as in (A) in a quench-chase-pulse experiment. H3K9me3 (green) and DAPI were used as markers for SAHF formation. Scale bar is 10 μm. (See also **Suppl. Fig. S3C-D**).

F. Graphics show fluorescent intensity profiles quantified by Image J along lines drawn through nuclei as shown in panel (E).

Figure 3: New H3.3 localizes in PML-NBs together with DAXX and ATRX in proliferating and senescent cells.

A. Fluorescent microscopy visualization of new H3.3 (TMR, red) after *in vivo* labelling of proliferating (empty) or senescent (Ras) MRC5 e-H3.3 cells in a quench-chase-pulse experiment. Co-staining with DAXX (green) and PML (cyan, pseudo-color) shows colocalization of new H3.3 with its chaperone DAXX in PML-NBs. Merge images represent PML in blue, DAXX in green, and new H3.3 (TMR) in red. Scale bar is 10 μm. (See also **Suppl. Fig. S4A-B**).

B. Graphics show fluorescent intensity profiles quantified using Image J along lines drawn through nuclei as shown in panel (A).

C. Fluorescent microscopy visualization of new H3.3 (TMR, red) after *in vivo* labelling of MRC5 e-H3.3 cells treated as in (A) in a quench-chase-pulse experiment. Co-staining with ATRX (green) and PML (cyan, pseudo-color) shows colocalization of new H3.3 with its chaperone ATRX in PML-NBs. Merge images represent PML in blue, ATRX in green, and new H3.3 (TMR) in red. Scale bar is 10 μm.

D. Graphics show fluorescent intensity profiles quantified by Image J along lines drawn through nuclei as shown in panel (C).

E. Immunoprecipitation performed against HA tag on 150μg of nuclear cell extracts from regular MRC5 cells (negative control) or MRC5 e-H3.1 or e-H3.3. Cells were either proliferating (empty) or induced into senescence by overexpression H-RasV12 (Ras) for 8 days. Input is 10% of the immunoprecipitated material. Membranes were probed for HA as a control for IP, for Mcm7 as a marker of cell proliferation and negative control for IP, and for DAXX and ATRX. M: molecular weight marker.

Figure 4: New H3.3 is lost from PML-NBs in DAXX-depleted cells.

A. Scheme for the assay of *in vivo* labeling of new H3.3 in MRC5 e-H3.3 induced into senescence and depleted of specific histone H3.3 chaperones.

B. Western blot analysis of total cell extracts from MRC5 e-H3.3 treated as in (A). Membranes were probed for HA and Ras to verify expression of the transduced proteins, and for DAXX and ATRX. Smc1 served as a loading control. M: molecular weight marker

C. Fluorescent microscopy visualization of new H3.3 (TMR, red) after *in vivo* labelling of MRC5 e-H3.3 cells treated as in (A) in a quench-chase-pulse experiment. Co-staining with PML (green) shows loss of new H3.3 at PML-NBs upon DAXX depletion. Insets represent enlarged images (3X) of selected area. Scale bar is 10 μm. (See also **Suppl. Fig. S7**).

D. Histogram shows quantitative analysis of the proportion of cells showing new H3.3 localization at PML-NBs. Numbers represent the mean of 3 independent experiments ± s.d.

Figure 5: Overexpression of DAXX increases new H3.3 localization at PML-NBs

A. (Left panel) Fluorescent microscopy visualization of new H3.3 (TMR, red) after *in vivo* labeling of MRC5 e-H3.3 cells in a quench-chase-pulse experiment. MRC5 e-H3.3 cells transduced with an empty vector (Empty) or a vector expressing Myc-DAXX (Myc-DAXX) were co-stained with Myc (green) and PML (cyan, pseudo-color). Scale bar is 10 μm. (Right panel) Graphics show distribution of new H3.3 (TMR) signal in MRC5 e-H3.3. TMR fluorescence intensity of each pixel delimited within the nuclei is plotted in a 3D-surface plot and shows increase in the targeting of new H3.3 at PML-NBs upon DAXX overexpression. (See also **Suppl. Fig. S10A**).

B. Western blot analysis of total cell extracts from MRC5 e-H3.3 treated as in (A) (left panel) or as in (C) (right panel). Membranes were probed for HA and Myc to verify expression of the transduced proteins, and for DAXX. α-Tubulin is a loading control. M: molecular weight marker.

C. (Left panel) Fluorescent microscopy visualization of new H3.3 (TMR, red) after *in vivo* labeling of MRC5 e-H3.3 cells in a quench-chase-pulse experiment. Control MRC5 e-H3.3

cells and MRC5 e-H3.3 cells co-expressing a siRNA resistant form of Myc-DAXX were transfected for 2 days with the indicated siRNAs before labeling with TMR and co-staining with Myc (green) and DAXX (cyan, pseudo-color). Scale bar is 10 μm. (Right panel) Graphics showing distribution of new H3.3 (TMR) signal intensity as in (A), reveals rescue of new H3.3 localization to PML-NBs upon re-expression of DAXX.

D. Histogram shows quantitative analysis of the proportion of cells showing new H3.3 localization at PML-NBs. Numbers represent the mean of 2 independent experiments ± s.d.

Figure 6: Overexpression of DAXX triggers formation of large PML-NBs together with an accumulation of HP1 proteins in these nuclear bodies.

A. Western blot analysis of total cell extracts from MRC5 cells transduced with an empty vector or a vector expressing Myc-DAXX. Membranes were probed for Myc to verify expression of the transduced proteins, and for DAXX. α-Tubulin is a loading control. M: molecular weight marker.

B. Fluorescent microscopy visualization of PML (green) and DAXX (red) in MRC5 cells treated as in (A) shows formation of large PML-NBs upon Myc-DAXX overexpression (white arrowheads). Scale bar is 10 μm.

C. Fluorescent microscopy visualization of nascent global RNA transcription *in vivo* in MRC5 cells empty or overexpressing Myc-DAXX. Nascent RNAs were labeled with 5-Ethynyl Uridine (EU) for 3 hours and revealed by the Click-iT chemistry (red). Co-staining with Myc (green) and PML (cyan, pseudo-color) shows absence of transcription within the large PML-NBs upon overexpression of DAXX. Insets represent enlarged images (3X) of selected area. Scale bar is 10 μm.

D and E. Fluorescent microscopy visualization of Myc-DAXX (Myc, green) and HP1γ or H3K9me3 (red) in MRC5 cells treated as in (A) shows accumulation of HP1γ **(D)** in absence

of H3K9me3 **(E)** in the large PML-NBs upon overexpression of Myc-DAXX (white arrowheads). Scale bar is 10 μm.

Figure 7: Enrichment of H3.3 in pericentromeric heterochromatin is dependent on DAXX and PML proteins

A. Histogram shows analysis of H3.3 incorporation in centromeric (Satellite α) or pericentromeric heterochromatin (Satellite III) by ChIP against the HA epitope in MRC5 e-H3.3 cells treated for 72h with the indicated siRNAs. QPCR data are presented as fold enrichment of IP over input DNA. MRC5 untransduced cells serve as a negative control. Numbers represent the mean of 2 independent experiments ± s.d.

B. Histogram shows analysis of H3.3 incorporation at the GAPDH promoter region by ChIP assay performed as in (A). Numbers represent the mean of 2 independent experiments ± s.d.

C. Western blot analysis of total cell extracts from MRC5 e-H3.3 cells treated as in (A). Membranes were probed for PML and DAXX to verify depletion of these proteins, and for HA to verify expression of the transduced proteins. α-Tubulin is a loading control. M: molecular weight marker.

D. Satellite III mRNA expression levels in empty MRC5 cells or MRC5 cells overexpressing Myc-DAXX as determined by quantitative RT-PCR. mRNA levels were normalized to the reference gene GAPDH and levels were set to 100% in empty cells. Numbers represent the mean of 3 independent experiments ± s.d.

E. Histogram shows analysis of H3.3 incorporation in centromeric (Satellite α) or pericentromeric heterochromatin (Satellite III) by ChIP against the HA epitope in MRC5 e-H3.3 cells transduced with an empty vector (empty) or a vector encoding Myc-DAXX (Myc-DAXX). QPCR data are presented as fold enrichment of IP over input DNA. IP with IgG

control antibody in MRC5 e-H3.3 cells serves as a negative control. Numbers represent the mean of 2 independent experiments ± s.d.

F. Histogram shows analysis of H3.3 incorporation at the GAPDH promoter region by ChIP assay performed as in (E). Numbers represent the mean of 2 independent experiments ± s.d.

Figure 1

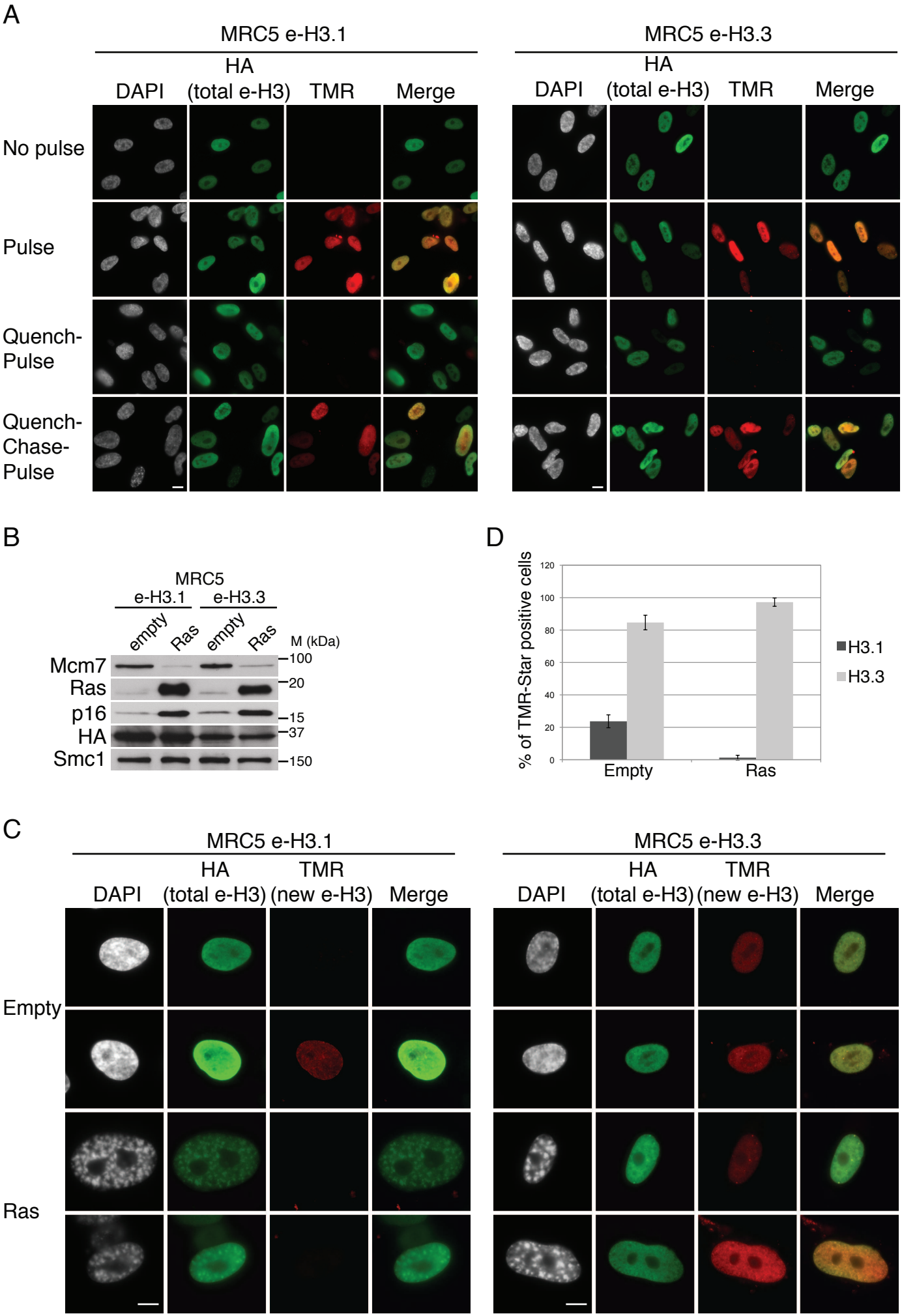
A
MRC5 e-H3.1
MRC5 e-H3.3
DAPI
HA (total e-H3)
TMR
Merge
No pulse
Pulse
Quench-Pulse
Quench-Chase-Pulse
B
MRC5
e-H3.1
e-H3.3
empty
Ras
empty
Ras
M (kDa)
Mcm7
Ras
p16
HA
Smc1
100
20
15
37
150
D
% of TMR-Star positive cells
120
100
80
60
40
20
0
Empty
Ras
H3.1
H3.3
C
MRC5 e-H3.1
MRC5 e-H3.3
DAPI
HA (total e-H3)
TMR (new e-H3)
Merge
Empty
Ras

Figure 2

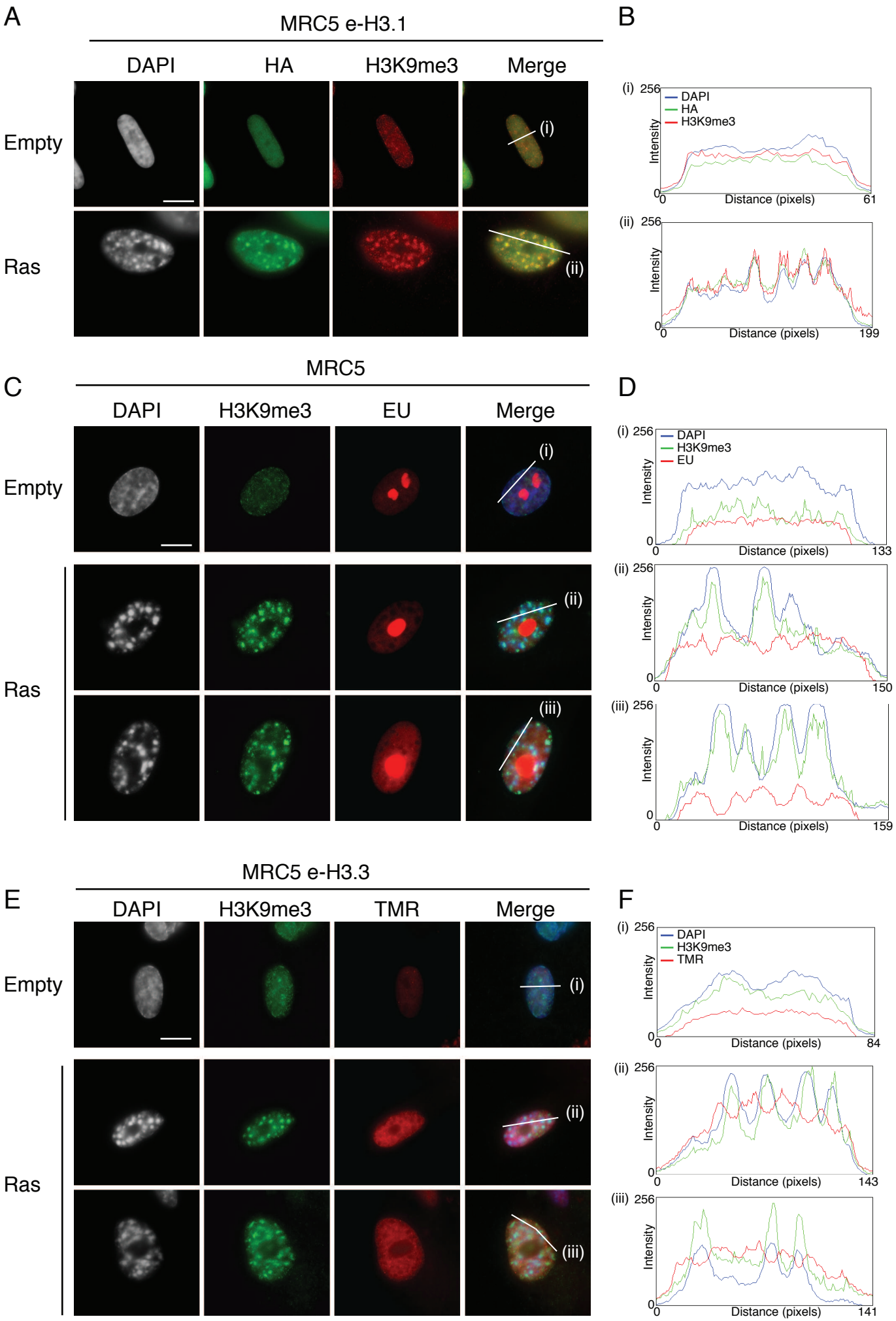
A
MRC5 e-H3.1
DAPI
HA
H3K9me3
Merge
Empty
Ras
(i)
(ii)
B
(i) 256
DAPI
HA
H3K9me3
Intensity
0
Distance (pixels)
61
(ii) 256
Intensity
0
Distance (pixels)
199
C
MRC5
DAPI
H3K9me3
EU
Merge
Empty
Ras
(i)
(ii)
(iii)
D
(i) 256
DAPI
H3K9me3
EU
Intensity
0
Distance (pixels)
133
(ii) 256
Intensity
0
Distance (pixels)
150
(iii) 256
Intensity
0
Distance (pixels)
159
E
MRC5 e-H3.3
DAPI
H3K9me3
TMR
Merge
Empty
Ras
(i)
(ii)
(iii)
F
(i) 256
DAPI
H3K9me3
TMR
Intensity
0
Distance (pixels)
84
(ii) 256
Intensity
0
Distance (pixels)
143
(iii) 256
Intensity
0
Distance (pixels)
141

Figure 3

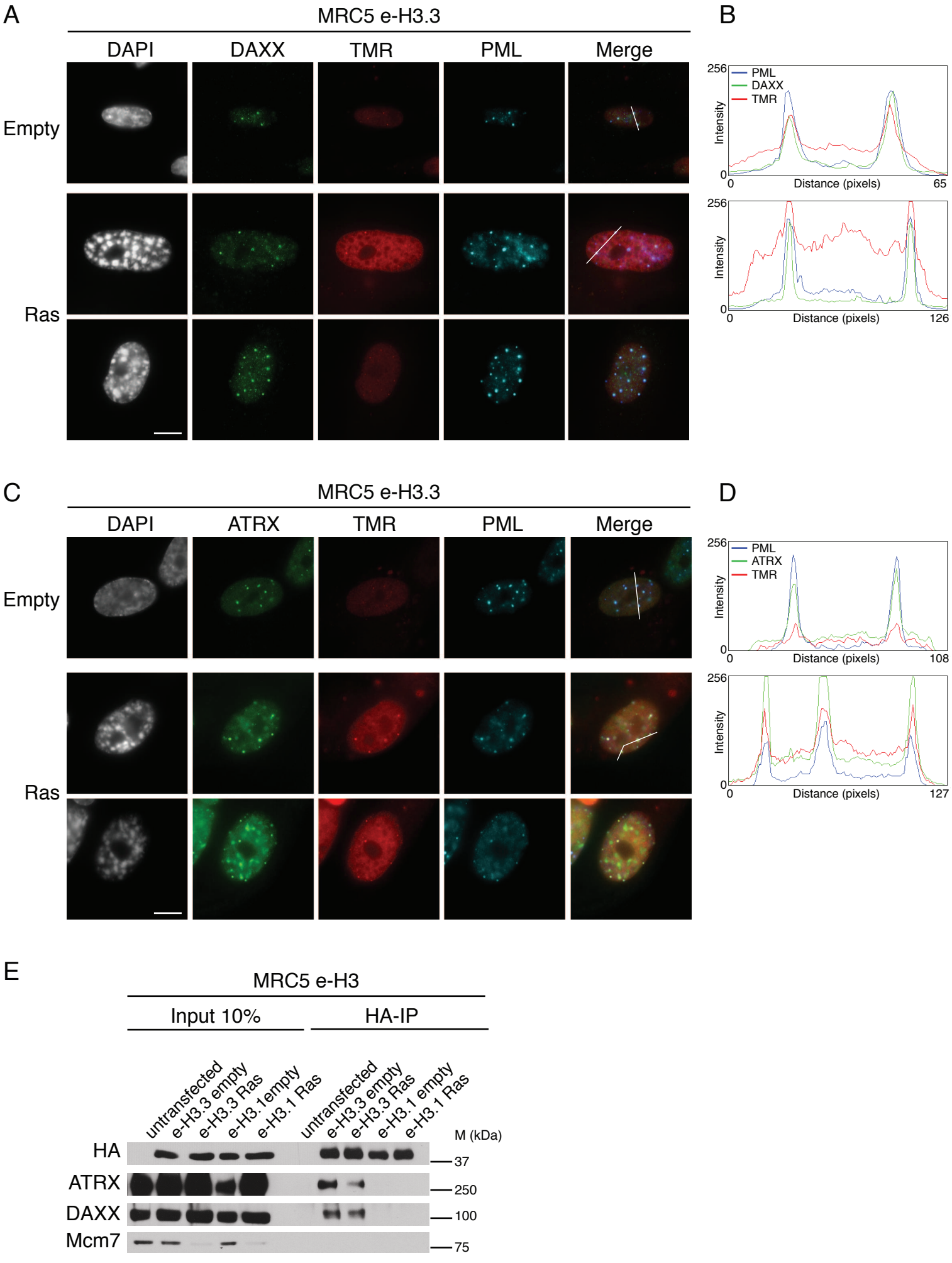
A
MRC5 e-H3.3
DAPI
DAXX
TMR
PML
Merge
Empty
Ras
B
PML
DAXX
TMR
Intensity
256
0
Distance (pixels)
65
126
C
MRC5 e-H3.3
DAPI
ATRX
TMR
PML
Merge
Empty
Ras
D
PML
ATRX
TMR
Intensity
256
0
Distance (pixels)
108
127
E
MRC5 e-H3
Input 10%
HA-IP
untransfected
e-H3.3 empty
e-H3.3 Ras
e-H3.1empty
e-H3.1 Ras
untransfected
e-H3.3 empty
e-H3.3 Ras
e-H3.1 empty
e-H3.1 Ras
M (kDa)
HA
ATRX
DAXX
Mcm7
37
250
100
75

Figure 4

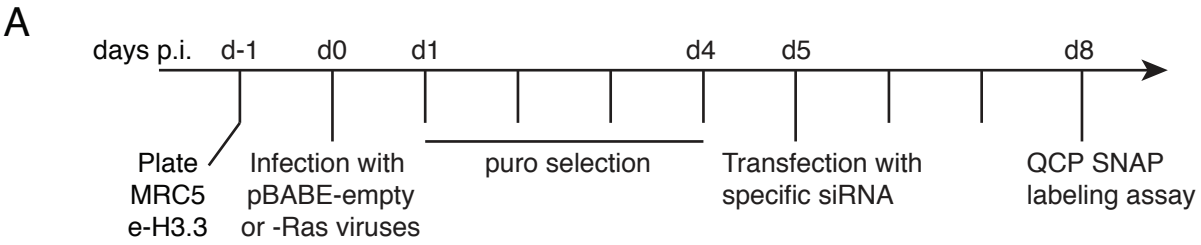
A
days p.i.
d-1
d0
d1
d4
d5
d8
Plate MRC5 e-H3.3
Infection with pBABE-empty or -Ras viruses
puro selection
Transfection with specific siRNA
QCP SNAP labeling assay

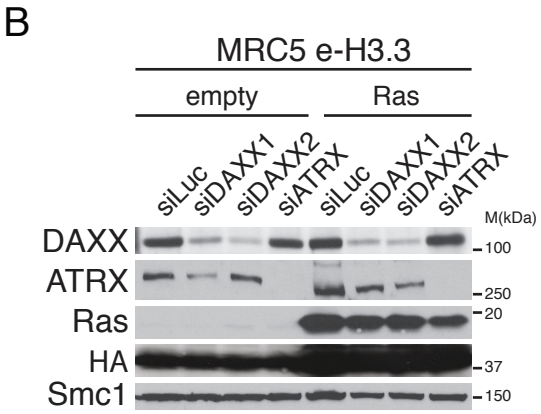
B
MRC5 e-H3.3
empty
Ras
siLuc
siDAXX1
siDAXX2
siATRX
siLuc
siDAXX1
siDAXX2
siATRX
M(kDa)
DAXX
ATRX
Ras
HA
Smc1
100
250
20
37
150

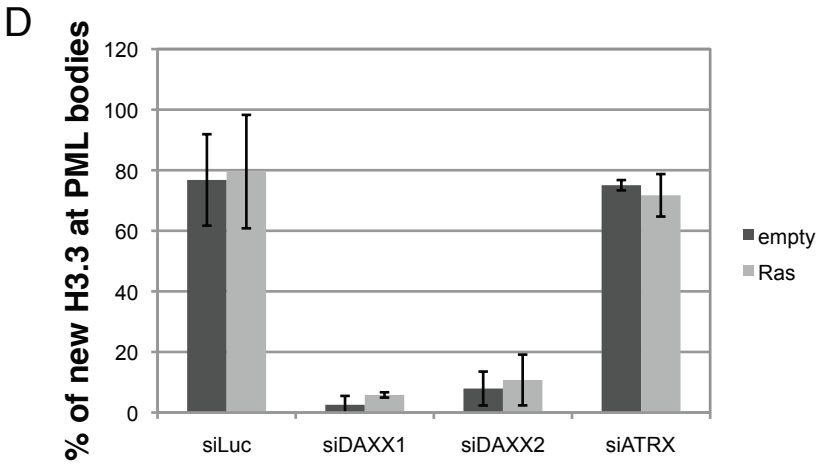
D
% of new H3.3 at PML bodies
120
100
80
60
40
20
0
siLuc
siDAXX1
siDAXX2
siATRX
empty
Ras

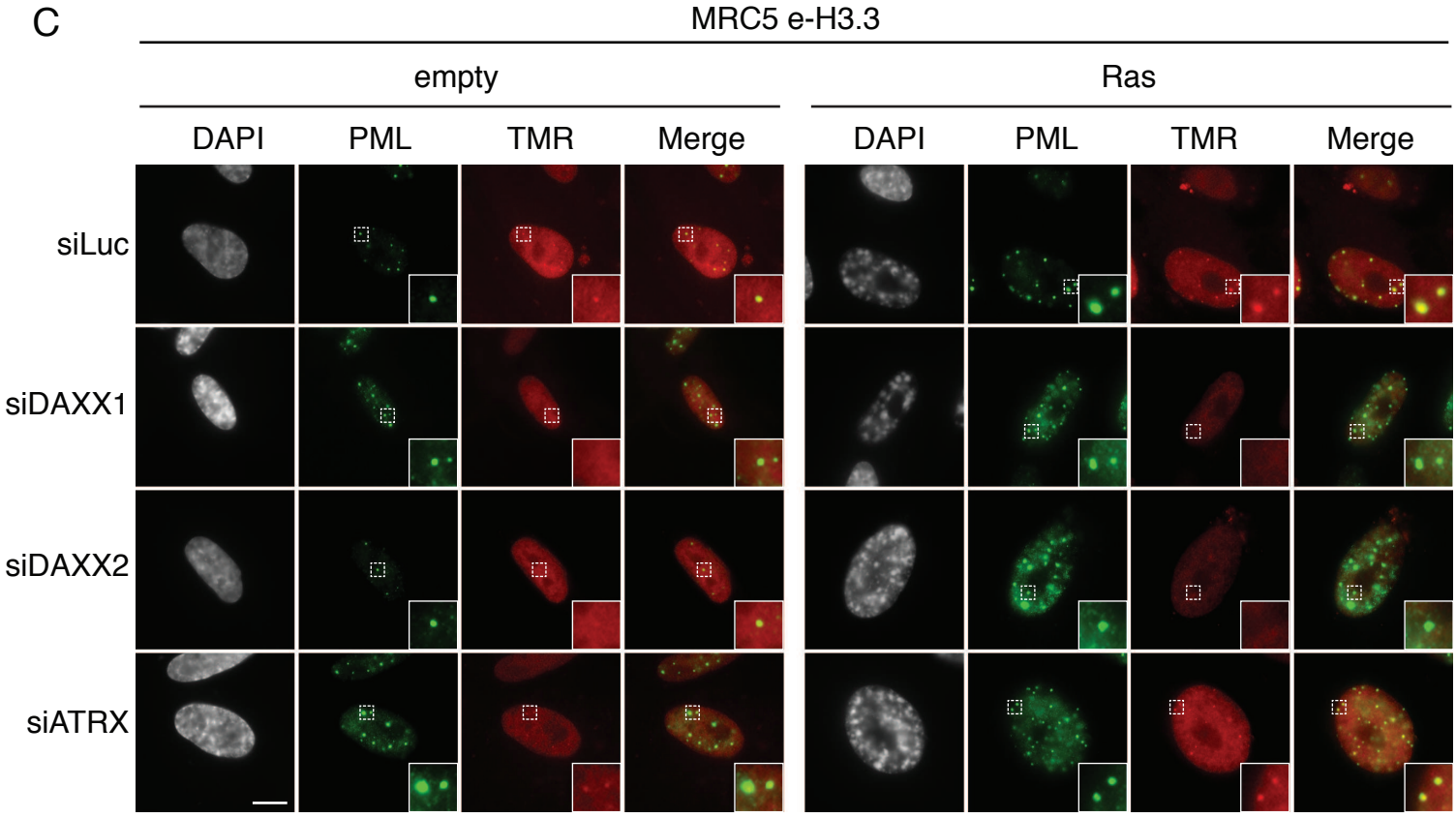
C
MRC5 e-H3.3
empty
Ras
DAPI
PML
TMR
Merge
DAPI
PML
TMR
Merge
siLuc
siDAXX1
siDAXX2
siATRX

Figure 5

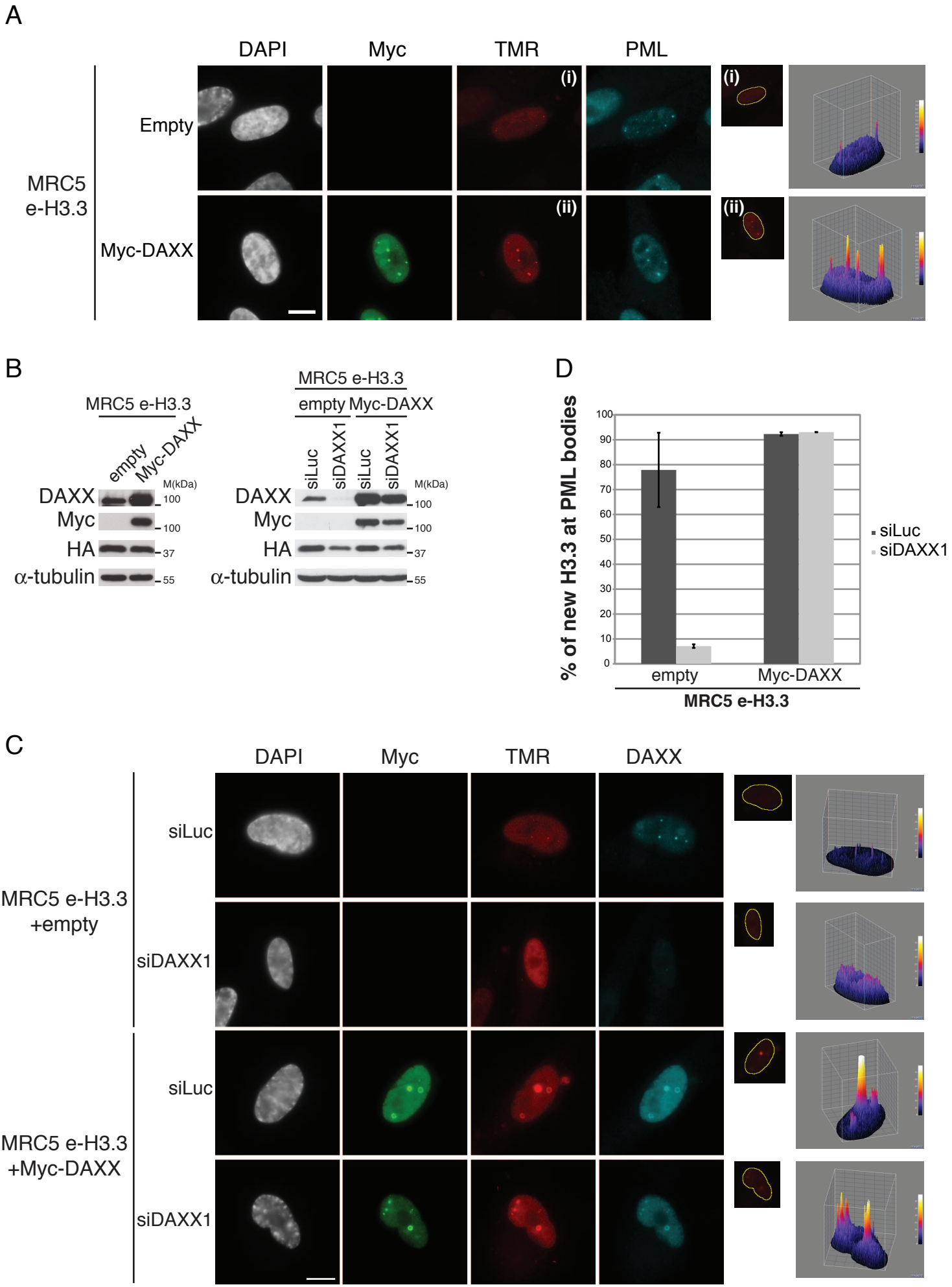
A
DAPI
Myc
TMR
PML
MRC5 e-H3.3
Empty
Myc-DAXX
(i)
(ii)
B
MRC5 e-H3.3
empty
Myc-DAXX
M(kDa)
DAXX
Myc
HA
α-tubulin
100
37
55
siLuc
siDAXX1
D
% of new H3.3 at PML bodies
empty
Myc-DAXX
MRC5 e-H3.3
siLuc
siDAXX1
C
DAPI
Myc
TMR
DAXX
MRC5 e-H3.3 +empty
MRC5 e-H3.3 +Myc-DAXX
siLuc
siDAXX1

Figure 6

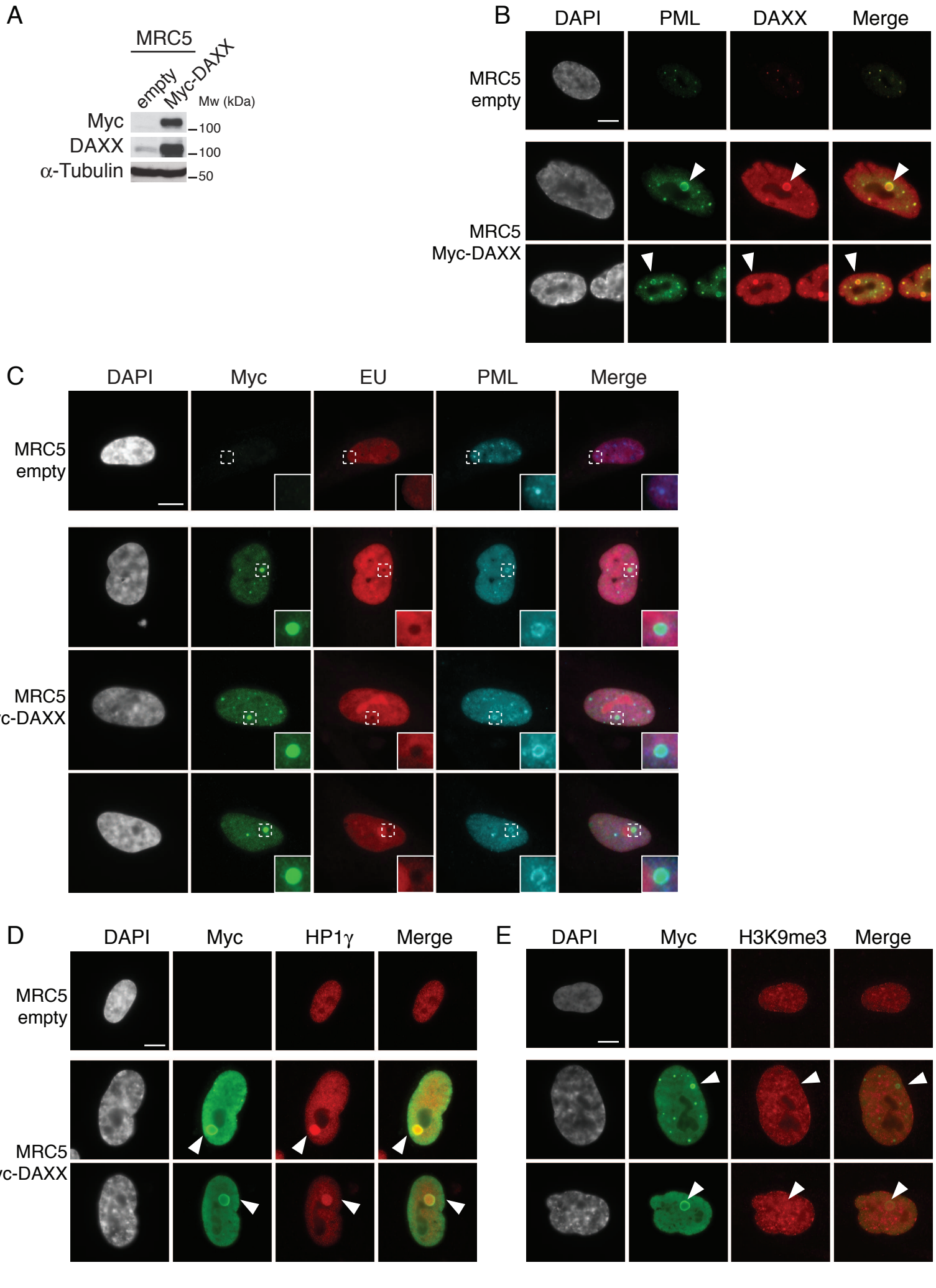
A
MRC5
empty
Myc-DAXX
Mw (kDa)
Myc
DAXX
α-Tubulin
100
100
50
B
DAPI
PML
DAXX
Merge
MRC5
empty
MRC5
Myc-DAXX
C
DAPI
Myc
EU
PML
Merge
MRC5
empty
MRC5
Myc-DAXX
D
DAPI
Myc
HP1γ
Merge
MRC5
empty
MRC5
Myc-DAXX
E
DAPI
Myc
H3K9me3
Merge

Figure 7

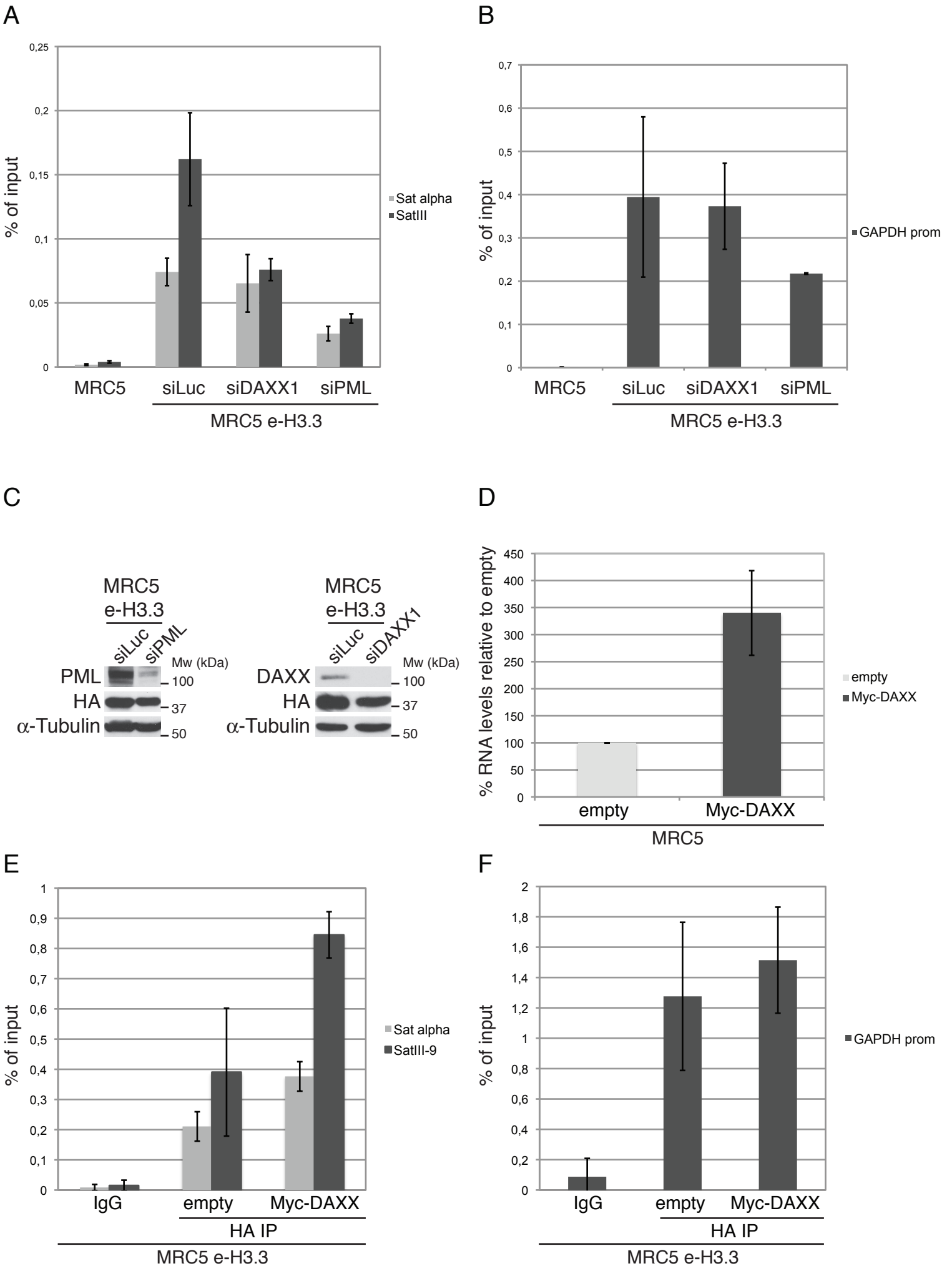
A
% of input
Sat alpha
SatIII
MRC5
siLuc
siDAXX1
siPML
MRC5 e-H3.3
B
% of input
GAPDH prom
MRC5
siLuc
siDAXX1
siPML
MRC5 e-H3.3
C
MRC5
e-H3.3
siLuc
siPML
Mw (kDa)
PML
HA
α-Tubulin
100
37
50
MRC5
e-H3.3
siLuc
siDAXX1
Mw (kDa)
DAXX
HA
α-Tubulin
100
37
50
D
% RNA levels relative to empty
empty
Myc-DAXX
MRC5
E
% of input
Sat alpha
SatIII-9
IgG
empty
Myc-DAXX
HA IP
MRC5 e-H3.3
F
% of input
GAPDH prom
IgG
empty
Myc-DAXX
HA IP
MRC5 e-H3.3

SUPPLEMENTARY INFORMATION

Dynamics of histone H3.3 deposition in proliferating and senescent cells reveals a DAXX-dependent targeting to PML-NBs important for pericentromeric heterochromatin organization

Authors:

Armelle CORPET*, Teresa OLBRICH, Myriam GWERDER, Daniel FINK and Manuel STUCKI*

Affiliation:

University Hospital Zürich, Departement of Gynecology, Wagistrasse 14, 8952 Schlieren, Switzerland.

* Corresponding authors:

Armelle Corpet: armelle.corpet@usz.ch, +41 44 556 30 46.

Manuel Stucki: manuel.stucki@usz.ch, +41 44 556 30 40.

Supplementary Materials and Methods

Immunofluorescence microscopy

For senescence-associated Beta-Gal assay, we followed protocols published in [1,2]. For detection of replicating cells 8 to 12 days after infection, we pulse-labeled cells in vivo with 10μM of BrdU (SIGMA) for 2 hours **(Fig. S2A)**. Alternatively, we pulse-labeled cells in vivo with 40μM of BrdU during the TMR-Star pulse labeling in the last 20 minutes **(Fig. S1C)**. In order to detect BrdU, we denatured fixed cells for 10 minutes in 4N HCl, followed by extensive washes in PBS and we then detected BrdU by standard immunofluorescence as described in main text.

Microscopy Analysis and Quantification of TMR Signal

We carried out confocal microscopy with a Leica SP5 confocal laser scanning microscope (Leica, Heerbrugg, Switzerland) equipped with a Plan-Apochromat 63x NA 1.4 oil immersion objective **(Fig. S3C)**. We acquired dual confocal images with standard settings using laser lines 488nm and 561nm for excitation of Alexa Fluor 488 and TMR-Star dyes respectively. We used band pass filters 498-552nm and 588-647nm to collect the emitted fluorescence signals. We imaged nuclear DAPI using excitation by 405nm laser and band pass filter 410-452nm. Images from **Fig. S3C** represent single confocal planes.

RNA extraction and Quantitative RT-PCR

We used the RNeasy mini kit (QIAGEN) for total RNA extraction. After treating 1μg of RNA with Turbo DNAse (AMBION, Life Technologies) according to the manufacturer's instructions. We then performed reverse transcription using MMLV reverse transcriptase (Promega) with 100ng of random primers (ABI, Life Technologies) per reaction, respectively.

For quantitative PCR analysis, we used the 96-well plate LightCycler 480 Real-time PCR system from Roche and the SYBR Green PCR Master mix (Roche). We checked the efficiency of each primer pair (sequences below) with four cDNA dilutions of a standart cDNA. We measured duplicates (ChIP) or triplicates (quantiative RT-PCR) in all experiments and we normalized the quantity of mRNA to the quantity of mRNA corresponding to the human Glyceraldehyde 3-phosphate dehydrogenase (GAPDH). As a control when measuring SatIII RNA levels, all quantitative RT-PCRs were also performed in control samples lacking reverse transcriptase. Primer pairs for the quantitative RT-PCRs were the following: H3.1-F 5'-GGTGCGAGAAATAGCTCAGG-3'; H3.1-R 5'- CAAAACAATTCACGCCCTCT-3'; H3.3A-F 5'- CCAGGAAGCAACTGGCTACA-3'; H3.3A-R 5'- ACCAGGCCTGTAACGATGAG-3'; H3.3B-F 5'- GGATTTCAAAACCGACCTGA-3'; H3.3B-R 5'-AGCCAACTGGATGTCTTTGG-3'; GAPDH-F 5'- GAGTCAACGGATTTGGTCGT-3'; GAPDH-R 5'- TTGATTTTGGAGGGATCTCG-3'; SatIII-F 5'-AATCAACCCGAGTGCAATCGAATGGAATCG-3'; SatIII-R 5'- TCCATTCCATTCCTGTACTCGG-3' [3].

For ChIP analysis, we used the following primer pairs: Satα-F 5'- TAGACAGAAGCATTCTCAGAAACT-3'; Satα-R 5'-TCCCGCTTCCAACGAAA TCCTCCAAAC-3' [4]; SatIII : same primer pair as for RT-PCR.

Supplementary References

1. Dimri GP, Lee X, Basile G, Acosta M, Scott G, Roskelley C, Medrano EE, Linskens M, Rubelj I, Pereira-Smith O. A biomarker that identifies senescent human cells in culture and in aging skin in vivo. Proc Natl Acad Sci USA 1995; 92:9363–9367.

2. Debacq-Chainiaux F, Erusalimsky JD, Campisi J, Toussaint O. Protocols to detect senescence-associated beta-galactosidase (SA-βgal) activity, a biomarker of senescent cells in culture and in vivo. Nature Protocols 2009; 4:1798–1806.

3. Zhu Q, Pao GM, Huynh AM, Suh H, Tonnu N, Nederlof PM, Gage FH, Verma IM. BRCA1 tumour suppression occurs via heterochromatin-mediated silencing. Nature 2011; 477:179–184.

4. Morozov VM, Gavrilova EV, Ogryzko VV, Ishov AM. Dualistic function of Daxx at centromeric and pericentromeric heterochromatin in normal and stress conditions. nucleus 2012; 3:

5. Ray-Gallet D, Woolfe A, Vassias I, Pellentz C, Lacoste N, Puri A, Schultz DC, Pchelintsev NA, Adams PD, Jansen LET, Almouzni G. Dynamics of Histone H3 Deposition In Vivo Reveal a Nucleosome Gap-Filling Mechanism for H3.3 to Maintain Chromatin Integrity. Molecular Cell 2011; 44:928–941.

6. Shav-Tal Y, Blechman J, Darzacq X, Montagna C, Dye BT, Patton JG, Singer RH, Zipori D. Dynamic sorting of nuclear components into distinct nucleolar caps during transcriptional inhibition. Molecular Biology of the Cell 2005; 16:2395–2413.

Supplementary Figures

Figure S1: In vivo labeling assays for H3-SNAP-HAx3 in MRC5 human primary cells

A. Scheme for the assays of in vivo labeling of H3-SNAP-HAx3 histones in Pulse, Quench-Pulse and Quench-Chase-Pulse experiments in vivo. The Pulse labels pre-existing H3-SNAP with red fluorescent TMR-Star, the Quench-Pulse quenches pre-existing H3-SNAP with non-fluorescent Block preventing their subsequent labeling with TMR-Star and the Quench-Chase-Pulse labels new H3-SNAP synthesized during the 3h30 chase. HA labels total histone H3. Adapted from [5].

B. Fluorescent microscopy visualization of total e-H3.1 and e-H3.3 (HA, green) colocalization with mitotic chromosomes in MRC5 cells. New H3.1 or H3.3 (TMR, red) were also labeled in vivo in a quench-chase-pulse experiment. During the chase period, new H3.3, but not H3.1, is incorporated in G2 phase cells which then subsequently entered into mitosis allowing detection of new H3.3 on mitotic chromosomes. DAPI stains nuclei. Scale bar is 10 μm.

C. Newly H3.1 is deposited during S-phase while H3.3 is deposited throughout the cell cycle. Fluorescent microscopy visualization of replication sites (BrdU, green) and of new H3.1 and H3.3 (TMR, red) after in vivo labeling in a quench-chase-pulse experiment. White and green arrowheads indicate typical negative and positive BrdU cells, respectively. DAPI stains nuclei. Scale bar is 10 μm.

D. Histogram shows the percentage of H3.1 and H3.3 cells negative (BrdU –) or positive (BrdU +) for BrdU staining which are labeled with TMR-Star. Error bars indicate the standard deviation of two independent experiments (n=200 nuclei counted per experiment).

Figure S2: New H3.3 is incorporated in oncogene-induced senescent MRC5 cells

A. Fluorescent microscopy visualization of proliferating (empty) or senescent (Ras) MRC5 cells labeled with BrdU (green). We fixed cells at day 8 post-infection. DAPI stains nuclei and is a marker of SAHF formation. Scale bar is 10 μm.

B. Conventional light microscopy vizualisation of a senescence associated Beta-Gal assay in MRC5 cells treated as in (A). Scale bar is 20μm.

C. Histograms show quantitative analysis of senescence induction in MRC5 cells. BrdU positive cells are a marker of cell proliferation (left panel), while cells positive for SAHF (middle panel) or SA-β-Gal (right panel) are markers of senescence entry. Numbers represent the mean of 2-3 independent experiments ± s.d.

D. Fluorescent microscopy visualization of new H3.1 and H3.3 (TMR, red) after *in vivo* labelling of MRC5 e-H3.1 and e-H3.3, transduced with an empty retroviral vector (empty) or with a vector expressing H-RasV12 (Ras) for 10 days, in a quench-chase-pulse experiment. Prior to fixation, soluble proteins were pre-extracted by detergent treatment (Triton) allowing detection of the incorporated histones only. HA (green) stains total H3 histones and DAPI stains nuclei. Of note, SAHF appear more fuzzy upon pre-extraction but H3.3 exclusion from SAHF is clearer. Scale bar is 10 μm.

Figure S3: H3.3 does not accumulate in SAHF in oncogene-induced senescent cells.

A. Quantitative RT-PCR analysis of H3.1, H3.3A and H3.3B mRNA levels in proliferating (empty) and senescent (Ras) MRC5 cells. We normalized levels to the reference gene GAPDH and set levels in proliferating cells to 100%. Error bars represent s.d. from 2 independent experiments.

B. Western blot analysis of fractionated cell extracts from MRC5 e-H3.1/e-H3.3, either proliferating (empty) or induced into senescence (Ras) for 9 days. 15μg of cytosolic (Cyt.) and nuclear salt-extractable (Nuc.) protein extracts and 25 μg of the chromatin pellet (Pellet)

were loaded. Mcm7 was used as a marker for cell proliferation and p16 as a marker for proliferation arrest. Membranes were probed for ATRX, DAXX, HIRA, ASF1a, H3.3 and Ras. Smc-1 and α-Tubulin served as loading controls. M: molecular weight marker.

C. Fluorescent confocal microscopy visualization of new H3.3 (TMR) after in vivo labeling of MRC5 e-H3.3 cells proliferating (empty) or induced into senescence with H-RasV12 overexpression (Ras) for 9 days in a quench-chase-pulse experiment. H3K9me3 and DAPI were used as markers for SAHF formation. Scale bar is 10 μm.

D. Fluorescent microscopy visualization of endogenous H3.3 (green) in IMR90 ER:Ras cells, non-induced (no 4-OHT) or induced into senescence with 4-OHT (+ 4-OHT) for 6 days. DAPI stains nuclei. Insets representing enlarged images (3X) of selected area underscore absence of H3.3 accumulation in SAHF. Scale bar is 10 μm.

Figure S4: H3.3 and its associated histone chaperones localize together in PML-NBs in proliferating and senescent cells

A. Fluorescent microscopy visualization of endogenous H3.3 (green) in IMR90 ER:Ras cells, non-induced (no 4-OHT) or induced into senescence with 4-OHT (+ 4-OHT) for 6 days. One day prior to addition of 4-OHT, cells were transfected with control siRNA (siLuc) or siRNAs targeting H3.3A and H3.3B (siH3.3). siRNA transfection was performed a second time after 3 days of 4-OHT. Absence of H3.3 staining in siH3.3 shows specificity of the antibody. PML (red) stains PML-NBs and DAPI stains nuclei. Insets representing enlarged images (3X) of selected area underscore localization of endogenous H3.3 in PML-NBs. Scale bar is 10 μm.

B. Fluorescent microscopy visualization of new H3.3 (TMR, red) after in vivo labeling of MRC5 e-H3.3 cells either proliferating (empty) or induced into senescence (Ras) in a quench-chase-pulse experiment. Co-staining with ASF1a (green) and HIRA (cyan, pseudo-color)

shows colocalization of new H3.3 with its chaperone ASF1a and HIRA in PML-NBs (white arrowheads). DAPI stains nuclei. Scale bar is 10 μm.

C. Fluorescent microscopy visualization showing colocalization of histone H3.3 chaperones ATRX, DAXX, ASF1a or HIRA (red) together with PML (green) in normal MRC5 cells, proliferating (empty) or induced into senescence (Ras) for 12 days. Numbers indicate the mean percentage of cells with colocalization of the histone H3.3 chaperone within PML-NBs ± s.d. from 2 independent experiments. DAPI stains nuclei. Scale bar is 10 μm.

Figure S5: DAXX-dependent localization of ATRX at PML-NBs

A. Western blot analysis of total cell extracts from MRC5 treated for 48h with the indicated siRNAs. Membranes were probed for ATRX, DAXX, HIRA (left panel) and H3.3 (right panel). α-Tubulin and Smc-1 served as loading controls. M: molecular weight marker.

B. Fluorescent microscopy visualization of ATRX (red, left panel) or DAXX (red, right panel) in MRC5 cells treated as in (A) showing loss of ATRX from PML-NBs (green) upon DAXX depletion. Insets represent enlarged images of selected area. DAPI stains nuclei. Scale bar is 10 μm.

Figure S6: ATRX localization to SAHF is increased in absence of DAXX

A. Fluorescent microscopy visualization of ATRX (green) in MRC5 e-H3.3 cells treated as in **Fig. 4A**. Western blot analysis is shown in **Fig. 4B**. DAPI stains nuclei and is a marker of SAHF. Scale bar is 10 μm.

B. Graphics show fluorescent intensity profiles quantified using Image J along lines drawn through nuclei as shown in panel (A). Comparison of profiles in proliferating (empty) cells treated with siLuc (i) or siDAXX1 (ii) shows loss of ATRX localization at PML-NBs upon DAXX depletion (see also **Fig. S5B**). In oncogene-induced senescent cells (Ras), ATRX

localization at PML-NBs increases (compare (iii) with (i)). Upon DAXX knockdown, ATRX localization to SAHF is increased (iv), since it is no longer targeted to PML-NBs.

Figure S7: H3.3 localization to PML-NBs in absence of PML or HIRA

A. Western blot analysis of total cell extracts from MRC5 e-H3.3 cells either proliferating (empty) or induced into senescence by H-RasV12 overexpression (Ras) for 7 days and treated with the indicated siRNAs during the last 48h. Membranes were probed for PML and Ras. Smc1 served as a loading control. M: molecular weight marker.

B. Fluorescent microscopy visualization of new H3.3 (TMR, red) after in vivo labeling of proliferating MRC5 e-H3.3 cells treated as in (A) in a quench-chase-pulse experiment. New H3.3 localization at PML-NBs is lost in absence of PML (green). Insets represent enlarged images (3x) of selected area. DAPI stains nuclei. Scale bar is 10 μm.

C. Histogram shows quantitative analysis of the proportion of cells showing new H3.3 localization at PML-NBs. Numbers represent the mean of 2 independent experiments ± s.d.

D. Western blot analysis of total cell extracts from MRC5 e-H3.3 cells treated as in (A). Membranes were probed for HIRA, Ras and HA. α-Tubulin served as a loading control. M: molecular weight marker.

E. Fluorescent microscopy visualization of new H3.3 (TMR, red) after in vivo labeling of MRC5 e-H3.3 cells treated as in (A) in a quench-chase-pulse experiment. New H3.3 localization at PML-NBs is not impaired in absence of HIRA. Insets represent enlarged images of selected area. DAPI stains nuclei. Scale bar is 10 μm.

F. Histogram shows quantitative analysis of the proportion of cells showing new H3.3 localization at PML-NBs. Numbers represent the mean of 2 independent experiments ± s.d.

Figure S8: Depletion of DAXX or ATRX or overexpression of DAXX in MRC5 cells does not impair senescence entry upon overexpression of H-RasV12

A. Fluorescent microscopy visualization of MRC5 cells cotransduced with a virus encoding HRas-V12 (Ras, green) and a virus encoding a control shRNA (pRetro empty) or a virus encoding a specific shRNA targeting DAXX (shDAXX1) or ATRX (shATRX1) for 8 days. DAPI stains nuclei and is a marker of SAHF. DAXX (left panel) or ATRX (right panel) are stained in red. Scale bar is 10 μm.

B. Histogram shows quantification of the mean number of positive cells for SAHF formation for cells treated as in (A). Error bars represent s.d. from 2 independent experiments.

C. Western blot analysis of total cell extracts from MRC5 treated as in (A). Membranes were probed for DAXX and Ras to verify expression of these proteins. Cyclin A was used as a marker for cell proliferation and p16 as a marker for proliferation arrest. α-Tubulin served as a loading control. The vertical bar indicates that a lane was cut from the gel. M: molecular weight marker.

D. Western blot analysis of total cell extracts from MRC5 empty cells or MRC5 overexpressing Myc-DAXX, transduced with an empty vector or with a vector expressing oncogenic Ras for 8 days. Membranes were probed for Myc, DAXX, and Ras to verify expression of the transduced proteins. Cyclin A was used as a marker for cell proliferation and p16 as a marker for proliferation arrest. α-Tubulin served as a loading control. M: molecular weight marker.

E. Fluorescent microscopy visualization of MRC5 cells treated as in (D). Myc (red) stains the epitope-tagged Myc-DAXX. DAPI stains nuclei and is a marker of SAHF. Scale bar is 10 μm.

Figure S9: Depletion of DAXX, ATRX or H3.3 in IMR90 ER:Ras does not impair senescence entry upon overexpression of H-RasV12

A. Scheme for the assay of induction into senescence in IMR90 ER:Ras. Cells were first transduced with a virus encoding a control shRNA (empty) or a virus encoding an shRNA against DAXX (shDAXX1) or ATRX (shATRX1). 5 days later, IMR90 ER:Ras were induced into senescence by addition of 4-OHT (100nM) and senescence was assessed 6 days after.

B. Immunofluorescence analysis of IMR90 ER:Ras treated as in (A). DAXX (red, left panel) or ATRX (red, right panel) proteins are depleted in the specific shRNAs. DAPI stains nuclei and is a marker of SAHF. Scale bar is 10 μm.

C. Histogram shows quantification of the mean number of positive cells for SAHF formation for cells treated as in (A). Error bars represent s.d. from 2 independent experiments.

D. Conventional light microscopy vizualisation of a senescence associated Beta-Gal assay in IMR90 ER:Ras cells treated as in (A). Scale bar is 20μm.

E. Western blot analysis of total cell extracts from IMR90 ER:Ras cells treated as in (A). In addition, IMR90 ER:Ras transduced with an empty virus (pLNCX2 empty) or a virus encoding Myc-DAXX (Myc-DAXX) were also included in the analysis of senescence induction with 4-OHT for 6 days. Membranes were probed for Myc, DAXX, and Ras to verify expression of the transduced proteins. Cyclin A was used as a marker for cell proliferation and p16 as a marker for proliferation arrest. α-Tubulin served as a loading control. M: molecular weight marker. The vertical bar indicates that a lane was cut from the gel. As shown on MRC5 cells in **Fig. S8**, depletion or overexpression of DAXX does not impair senescence entry.

F. Western blot analysis of total cell extracts from IMR90 ER:Ras cells, non-induced (no 4-OHT) or induced into senescence with 4-OHT (+ 4-OHT) for 6 days. One day prior to addition of 4-OHT, cells were transfected with control siRNA (siLuc) or siRNAs targeting

DAXX (siDAXX1 or siDAXX3), ATRX (siATRX1) or H3.3A and H3.3B (siH3.3). siRNA transfection was performed a second time after 3 days of 4-OHT. Membranes were probed for ATRX, DAXX, H3.3 and Ras to verify expression of these proteins. Cyclin A was used as a marker for cell proliferation and p16 as a marker for proliferation arrest. α-Tubulin served as a loading control. M: molecular weight marker.

G. Histogram shows quantification of the mean number of positive cells for SAHF formation for cells treated as in (F). Error bars represent s.d. from 2 independent experiments.

H. Fluorescent microscopy visualization of IMR90 ER:Ras cells treated as in (F). Addition of 4-OHT (+4-OHT) triggers accumulation of HRas-V12 (green) and senescence induction. DAPI stains nuclei and is a marker of SAHF. DAXX or ATRX are stained in red. Arrowheads indicate ATRX localization at SAHF. Scale bar is 10 μm. See also **Fig. S4A** for immunofluorescence analysis of siH3.3 treated cells.

Figure S10: Overexpression of DAXX triggers accumulation of new H3.3 in PML-NBs

A. (Left panel) Fluorescent microscopy visualization of new H3.3 (TMR, red) after *in vivo* labelling of MRC5 e-H3.3 cells transduced with an empty vector (Empty) or a vector expressing Myc-DAXX (Myc-DAXX) and co-stained with Myc (green) and DAXX (cyan, pseudo-color). Scale bar is 10 μm. (Right panel) Graphics show distribution of new H3.3 (TMR) signal in MRC5 e-H3.3. TMR fluorescence intensity of each pixel delimited within the nuclei is plotted in a 3D-surface plot shows increase of targeting of H3.3 at PML-NBs upon DAXX overexpression.

B. Fluorescent microscopy visualization of new H3.3 (TMR, red) after *in vivo* labelling of proliferating (empty) or senescent (Ras) MRC5 e-H3.3 cells in a quench-chase-pulse experiment. Prior to fixation, soluble proteins were pre-extracted by detergent treatment (Triton) allowing detection of the triton-insoluble proteins only. Co-staining with H3K9me3

(green) and PML (cyan, pseudo-color) shows colocalization of new triton-insoluble H3.3 within the PML-NBs and exclusion from SAHF, marked as H3K9me3 dense regions. Scale bar is 10 μm.

Figure S11: New H3.3 localizes in PML-NBs in nucleolar caps upon transcription inhibition.

A. Fluorescent microscopy visualization of new H3.3 (TMR, red) after *in vivo* labelling of MRC5 e-H3.3 in a quench-chase-pulse experiment. Cells were treated with DMSO or with Actinomycin D (ActD) at a dose of 2μg/mL for the total lenght of the chase (3h30) to prevent transcription of new H3.3 (control, no TMR signal), or for the end of the chase (1h30) to allow synthesis of new H3.3 before transcription inhibition. In this latter case, new H3.3 relocalizes together with PML in nucleolar caps as shown previously for PML upon transcription inhibition [6]. Insets represent enlarged images (3X) of selected area. PML (green) stains PML-NBs and DAPI stains nuclei. Scale bar is 10 μm.

B. Fluorescent microscopy visualization of new H3.3 (TMR, red) as in **A**. MRC5 e-H3.3 were transduced with an empty retroviral vector (empty) or with a vector expressing H-RasV12 (Ras) for 7 days. Actinomycin D (ActD) at a dose of 2μg/mL was added during the end of the chase (1h30). Insets represent enlarged images (3X) of selected area. PML (green) stains PML-NBs and DAPI stains nuclei. Scale bar is 10 μm.

Supplementary Figure S1

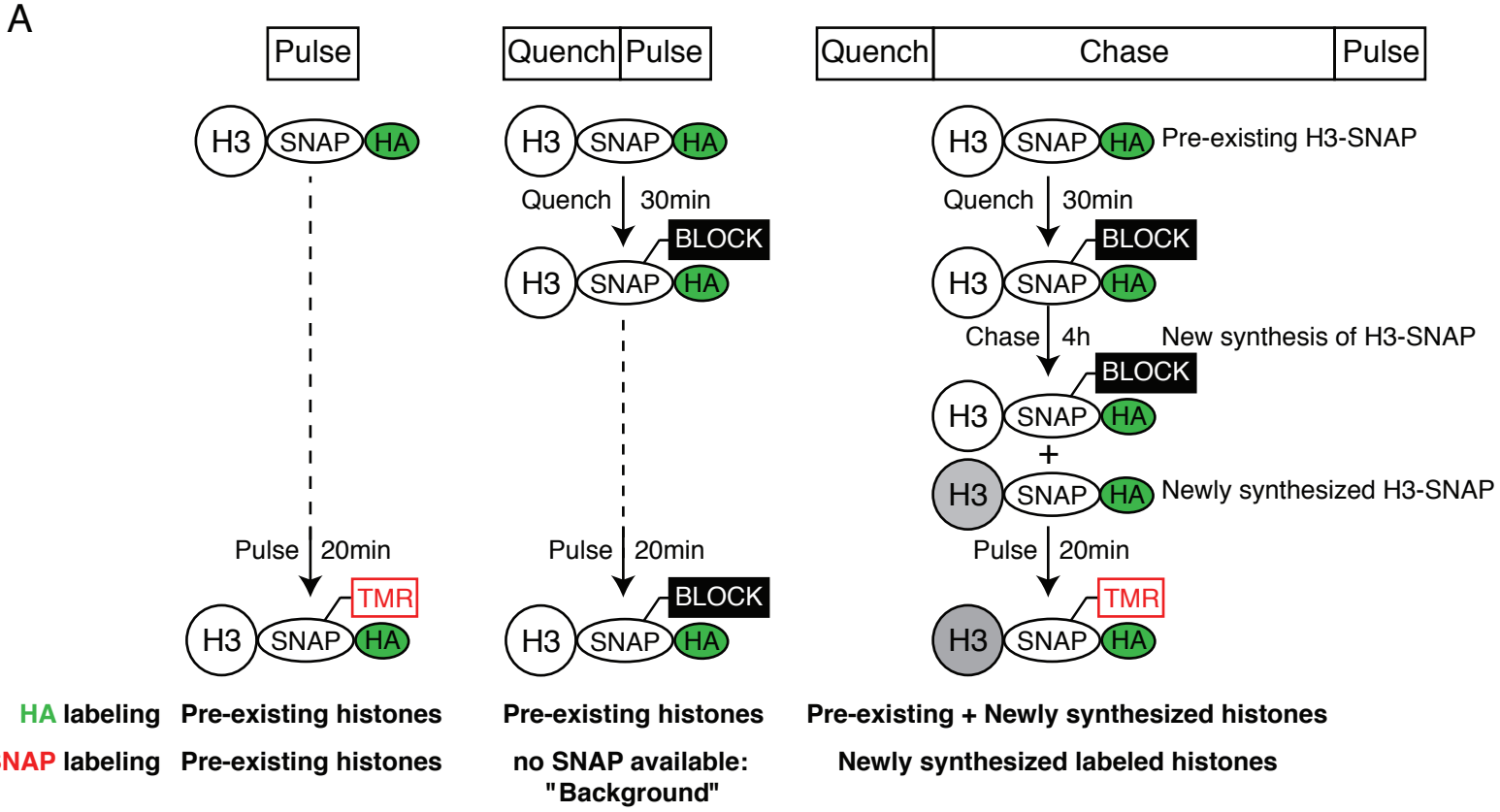

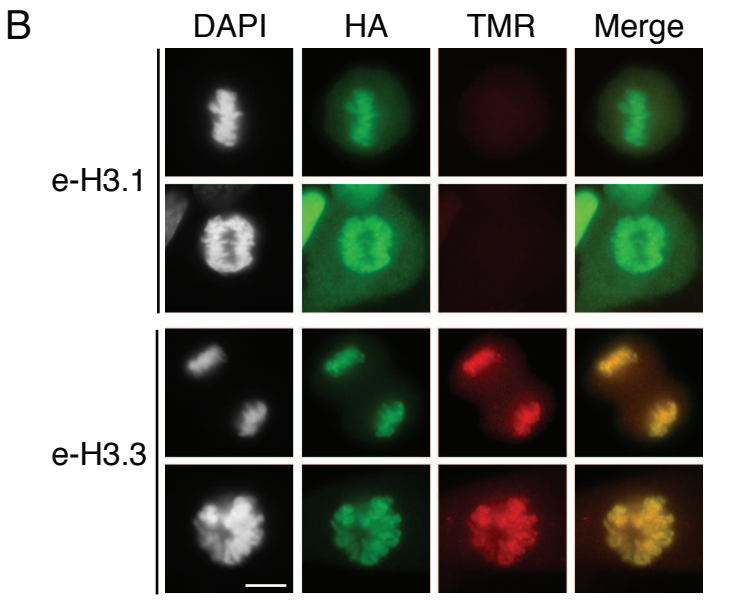

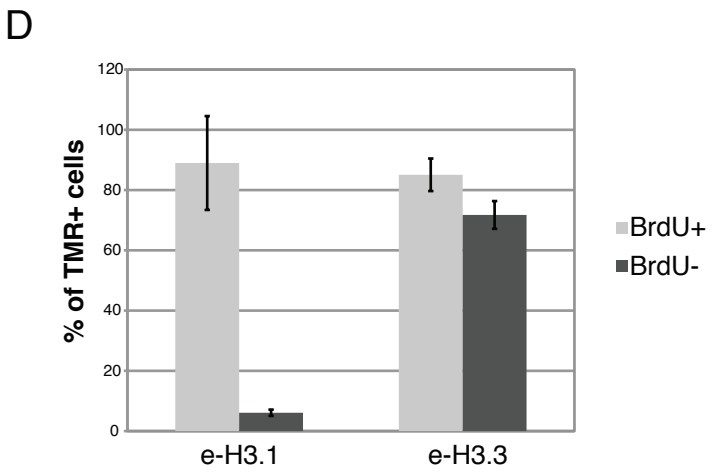

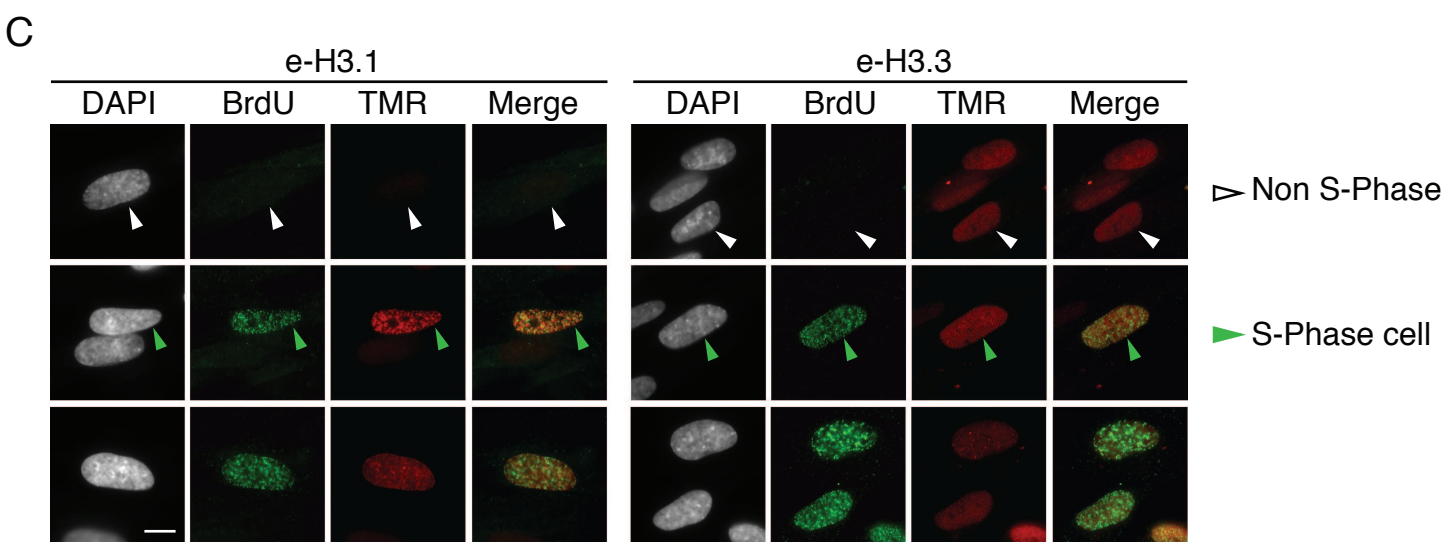

Supplementary Figure S2

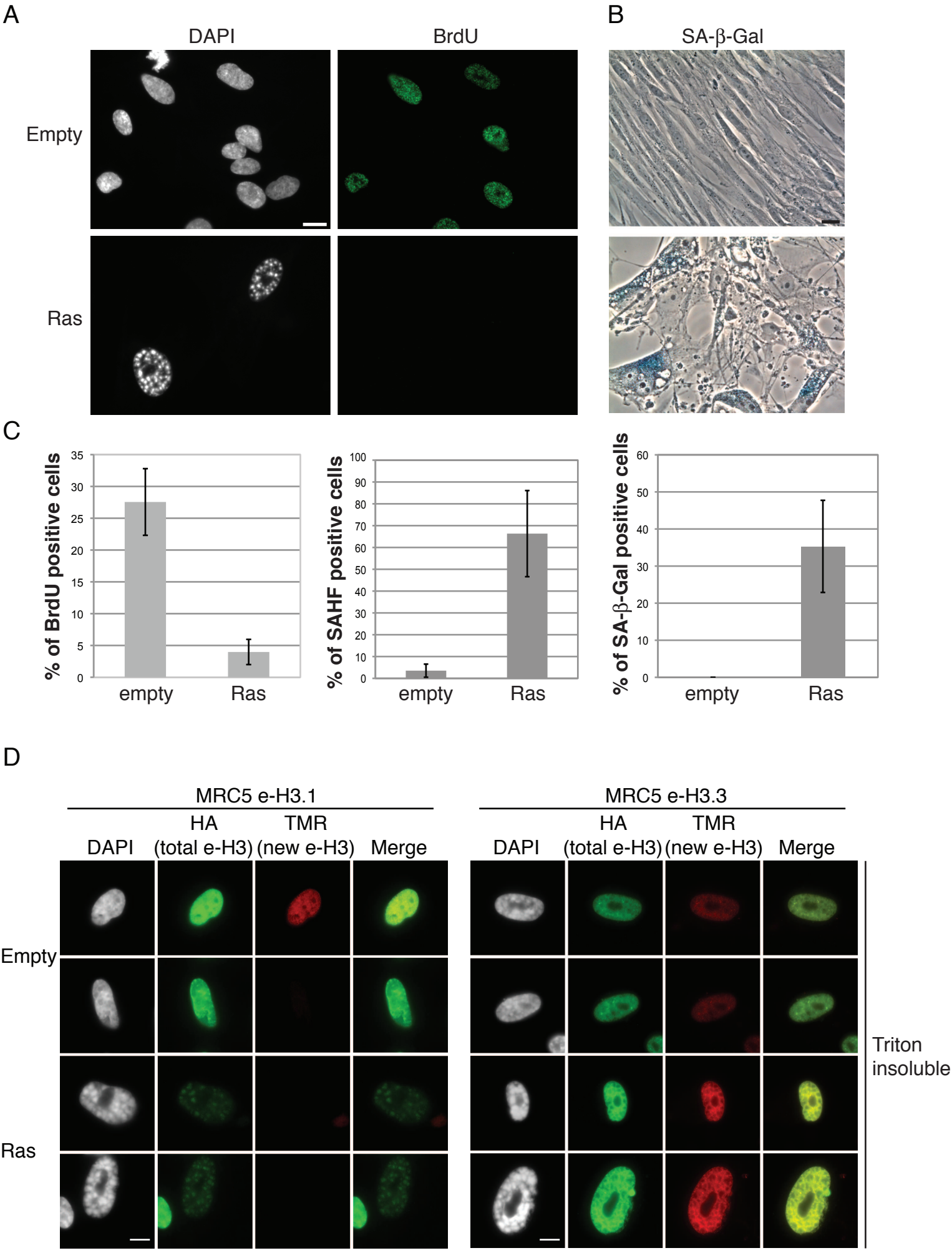

Supplementary Figure S3

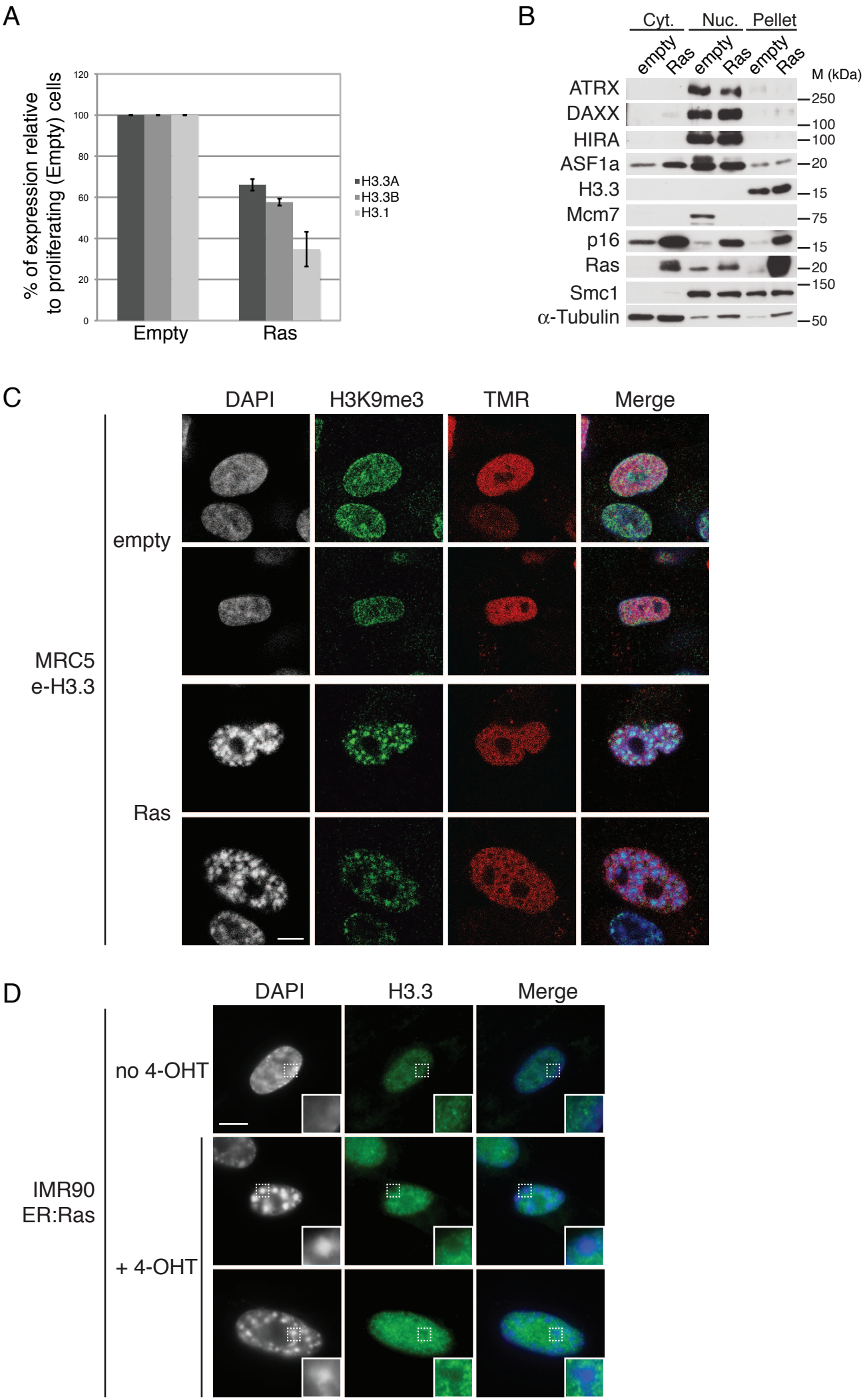

Supplementary Figure S4

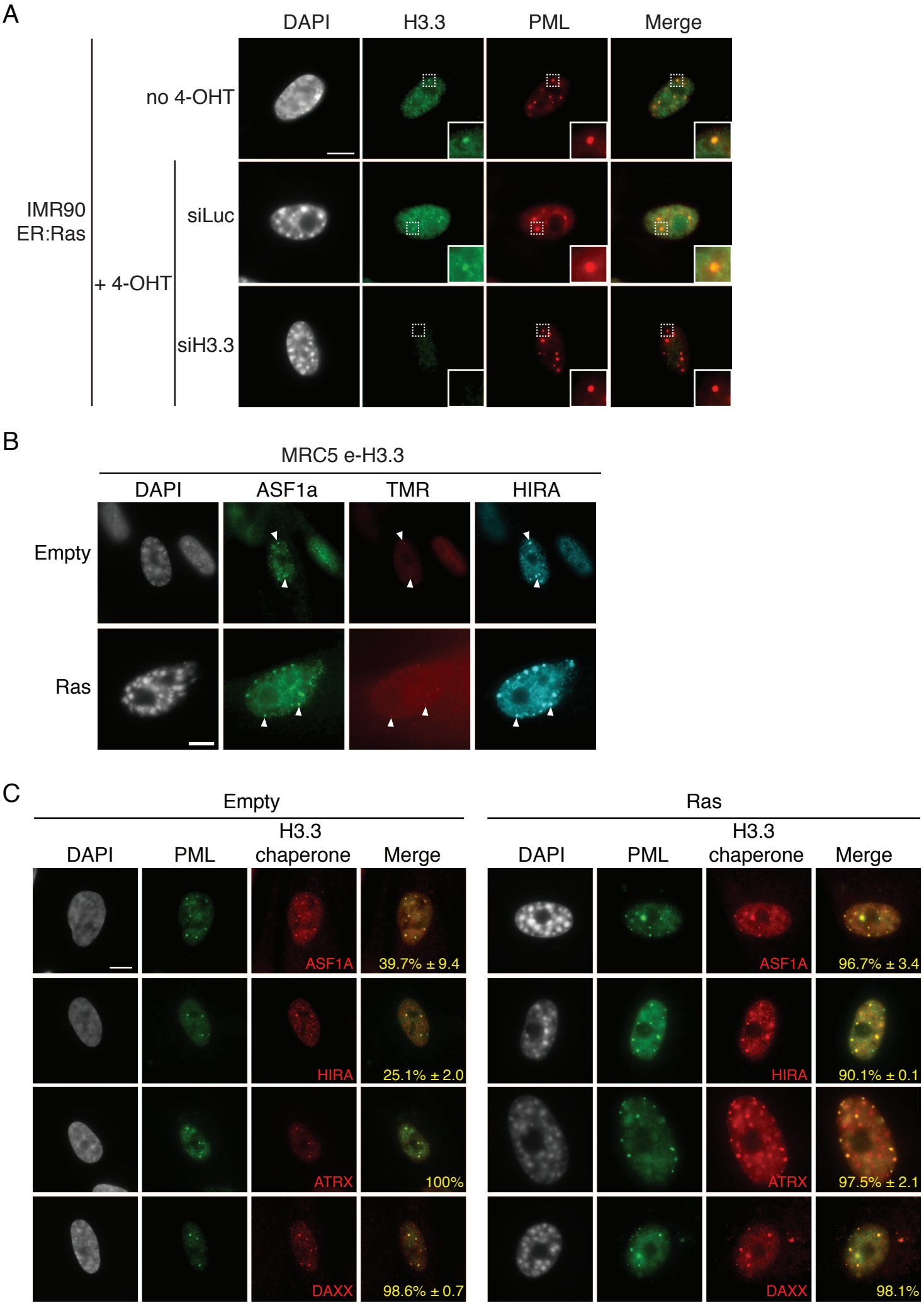

Supplementary Figure S5

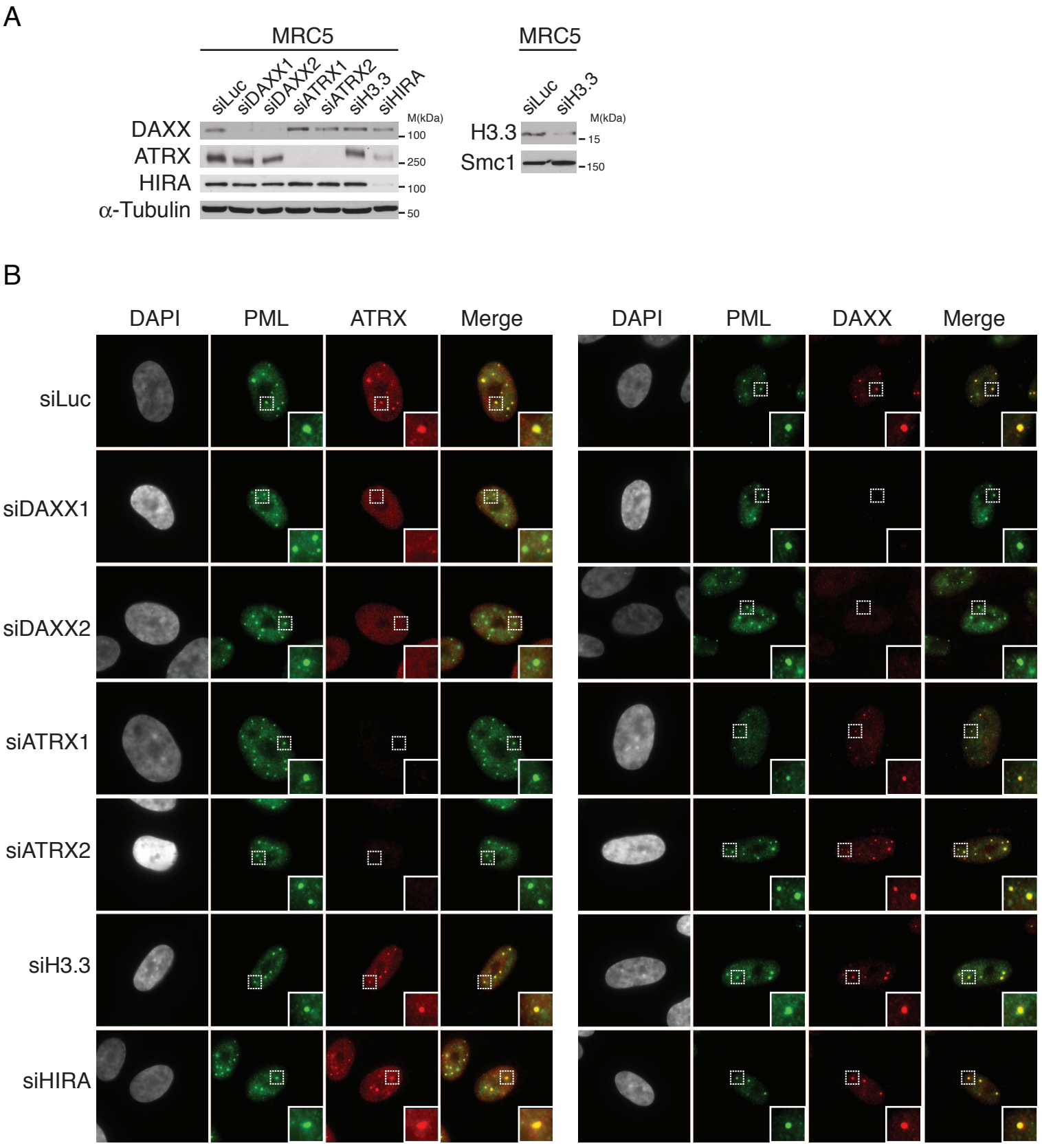

Supplementary Figure S6

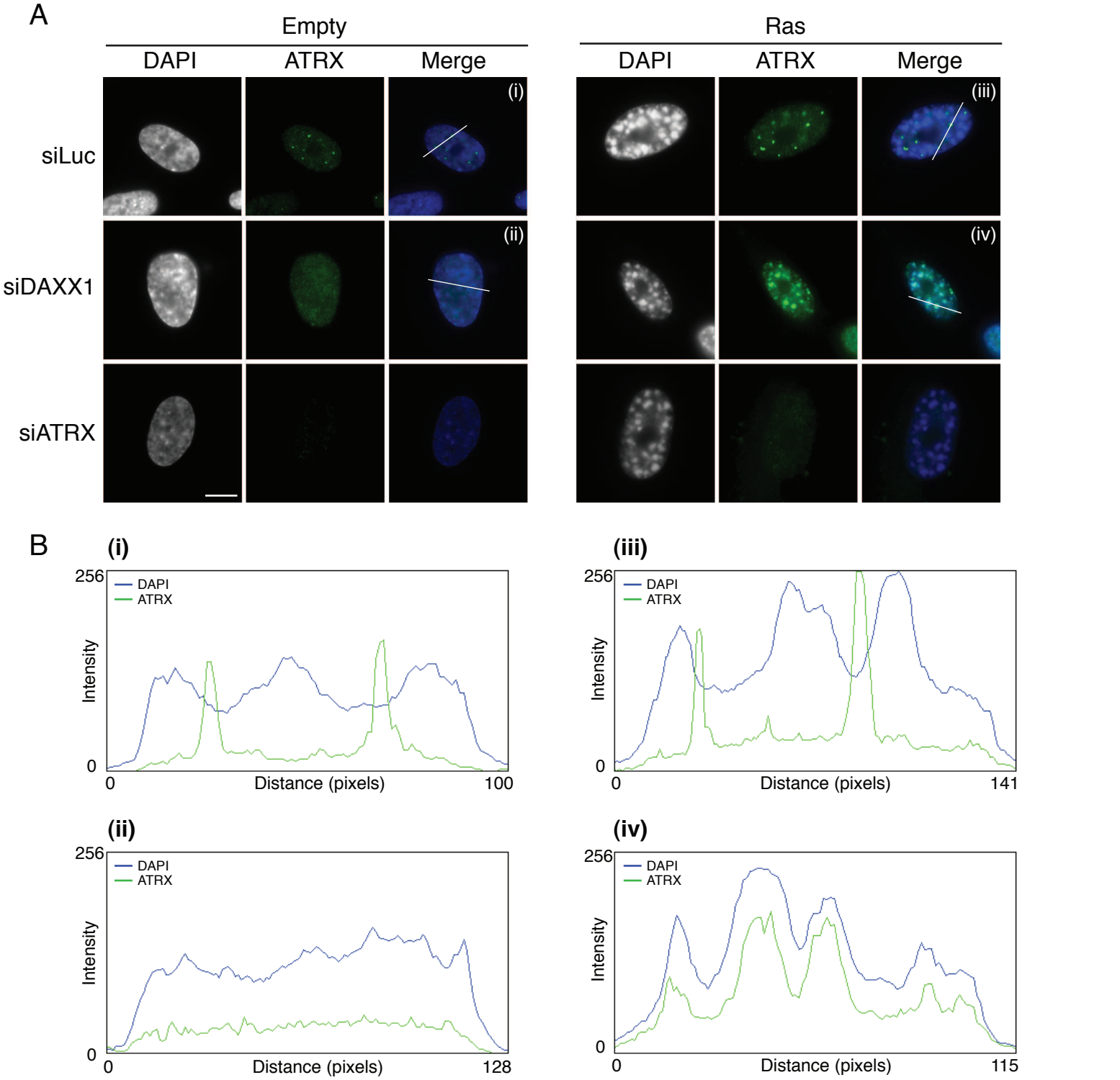

Supplementary Figure S7

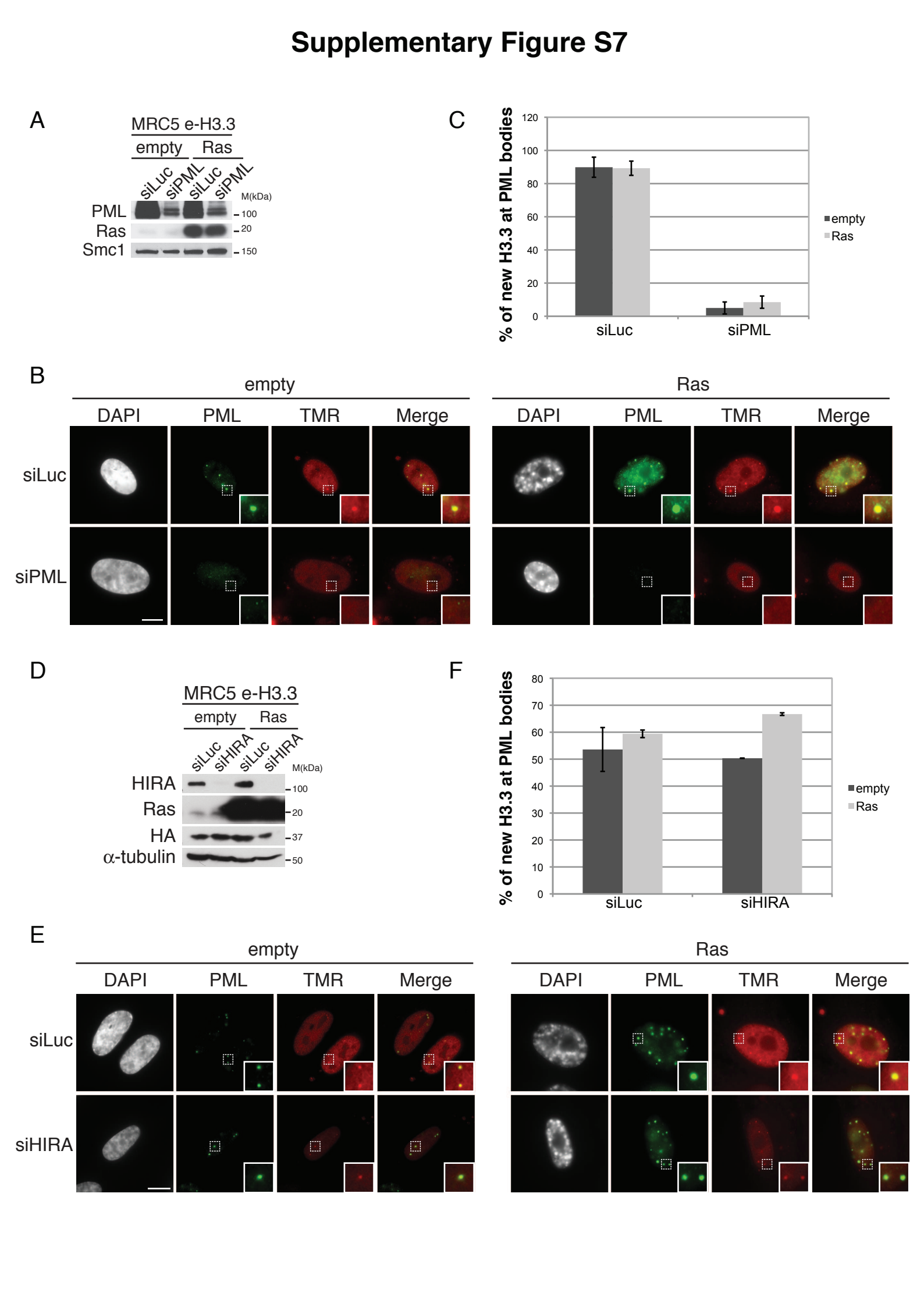

Supplementary Figure S8

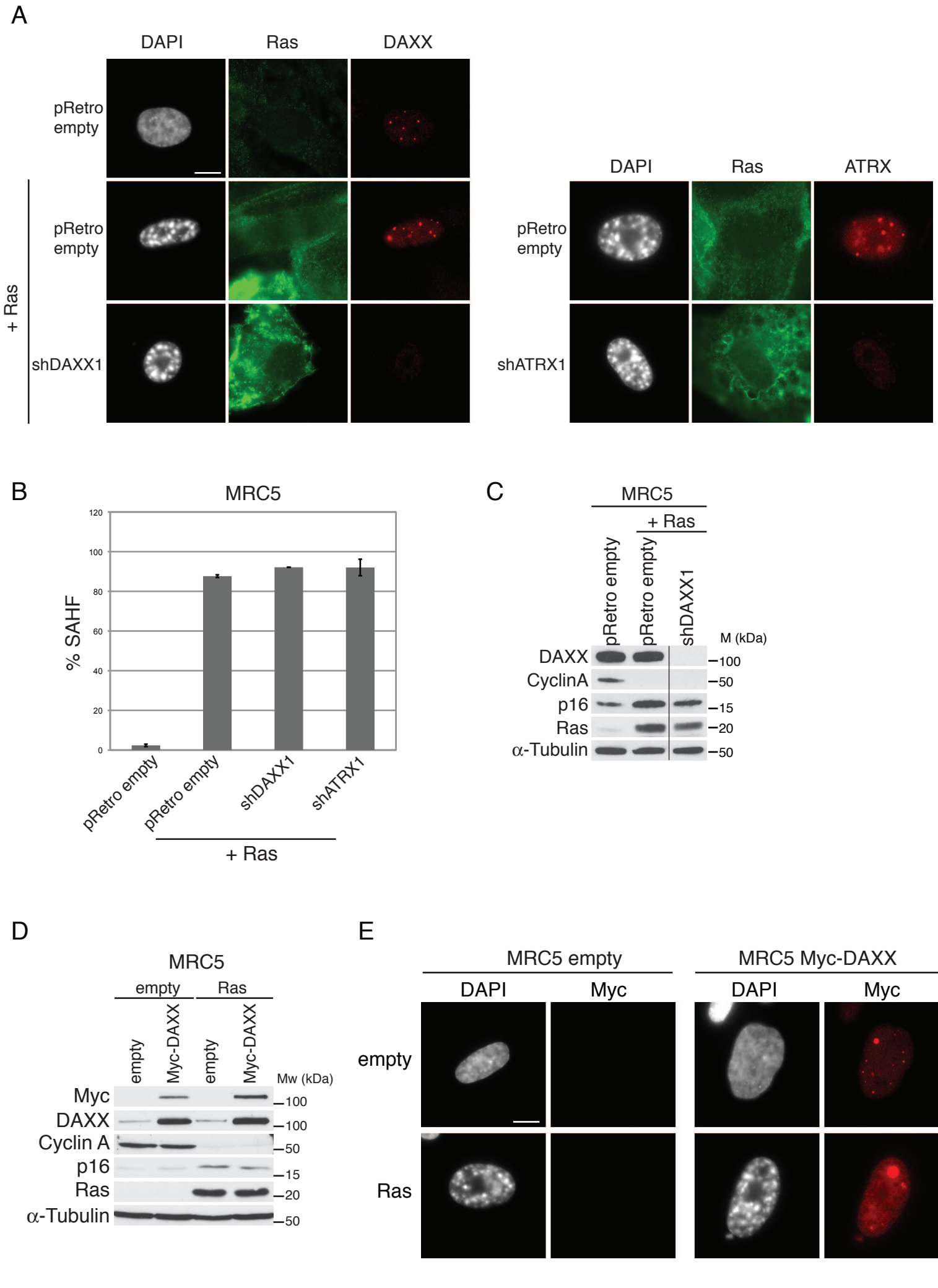

Supplementary Figure S9

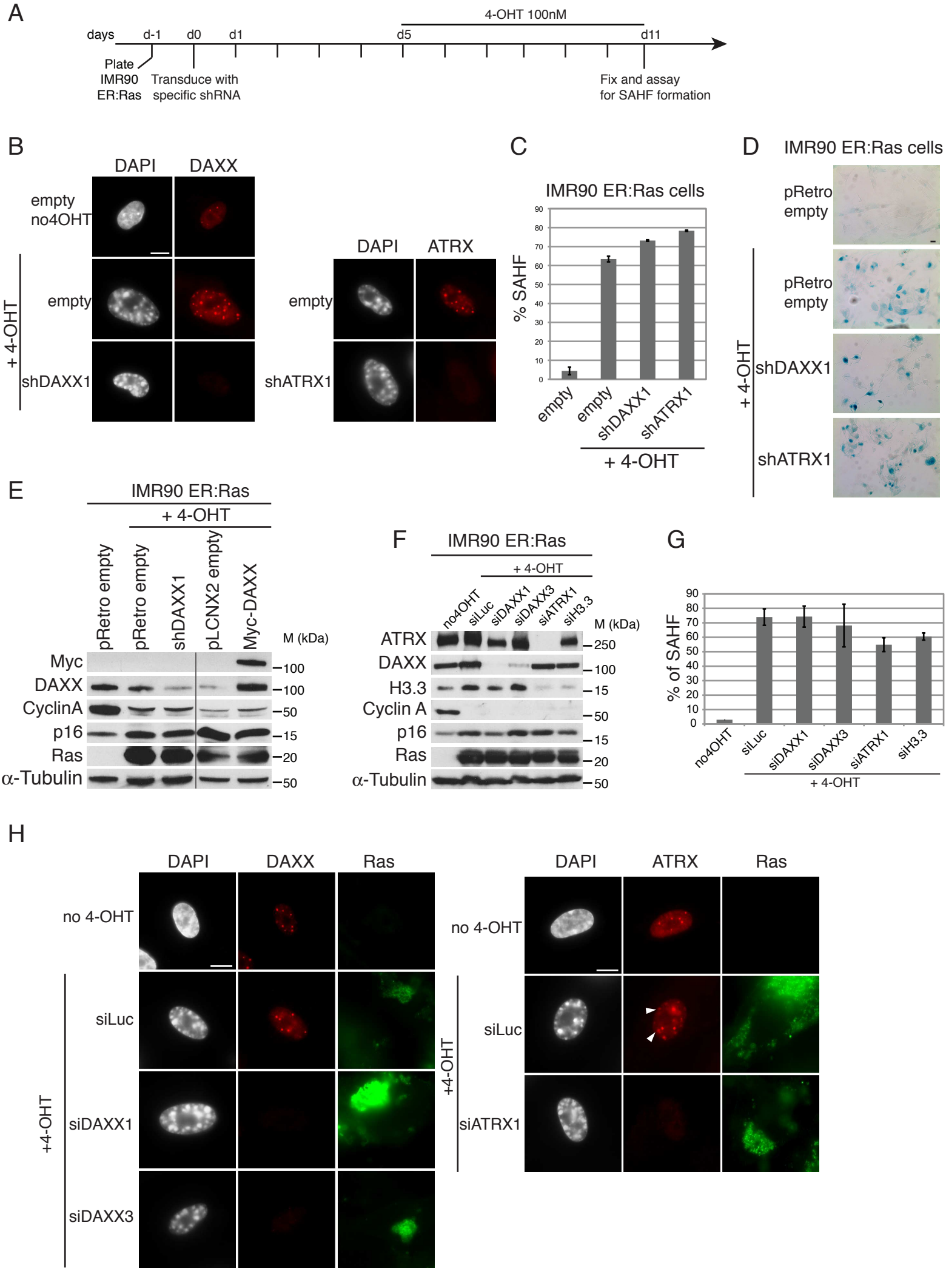

Supplementary Figure S10

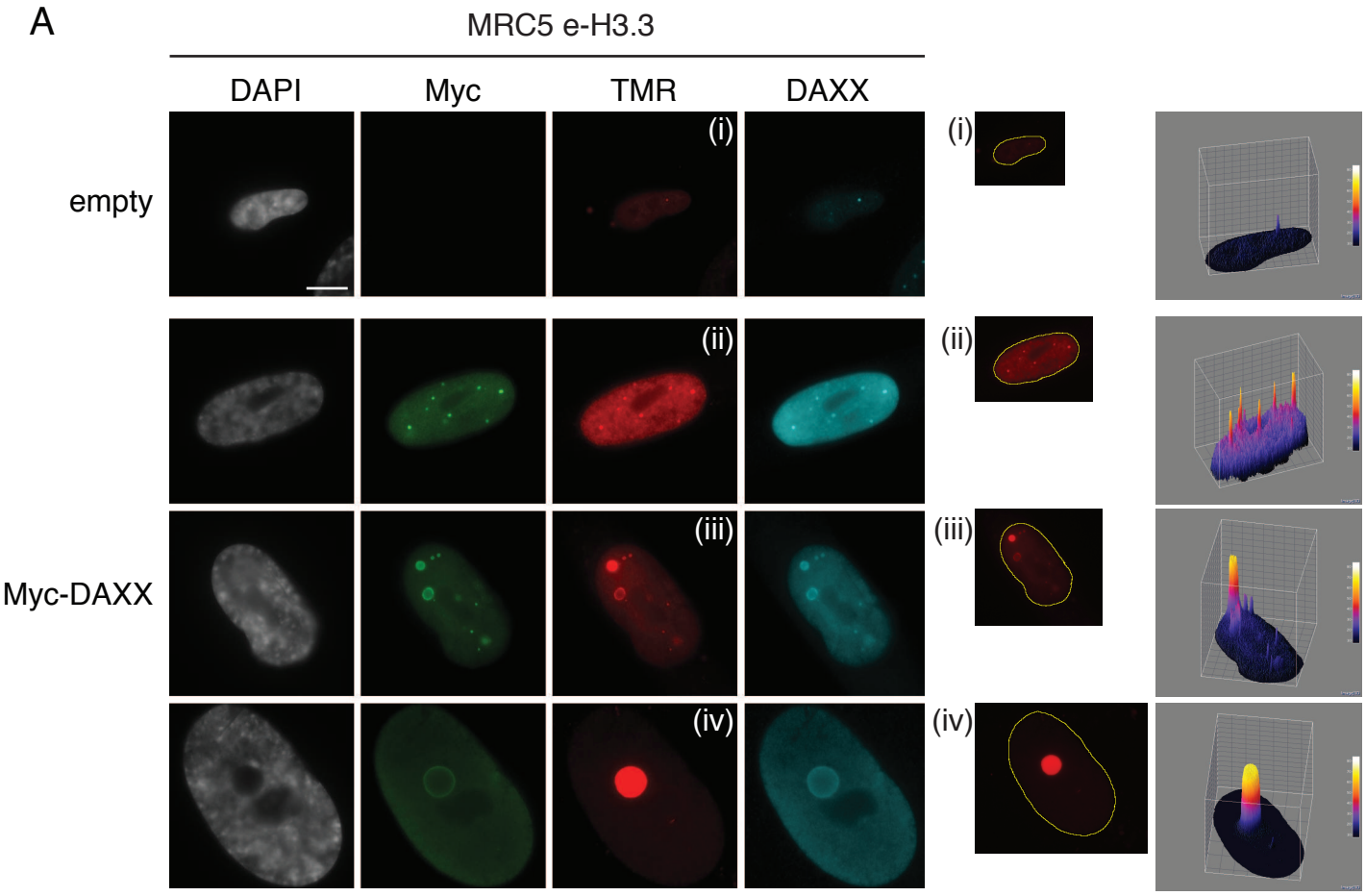

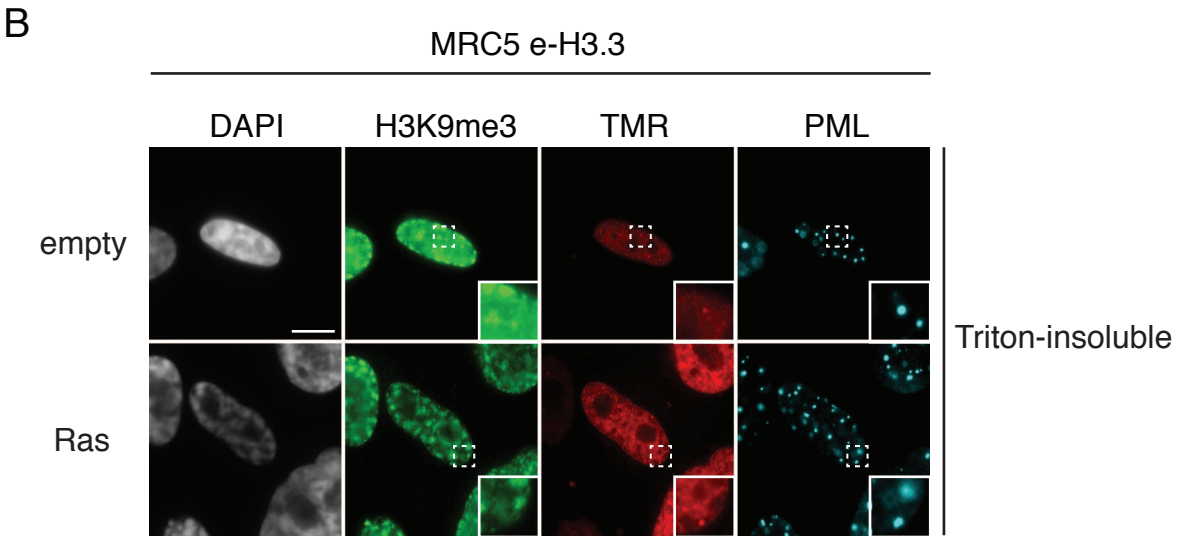

Supplementary Figure S11

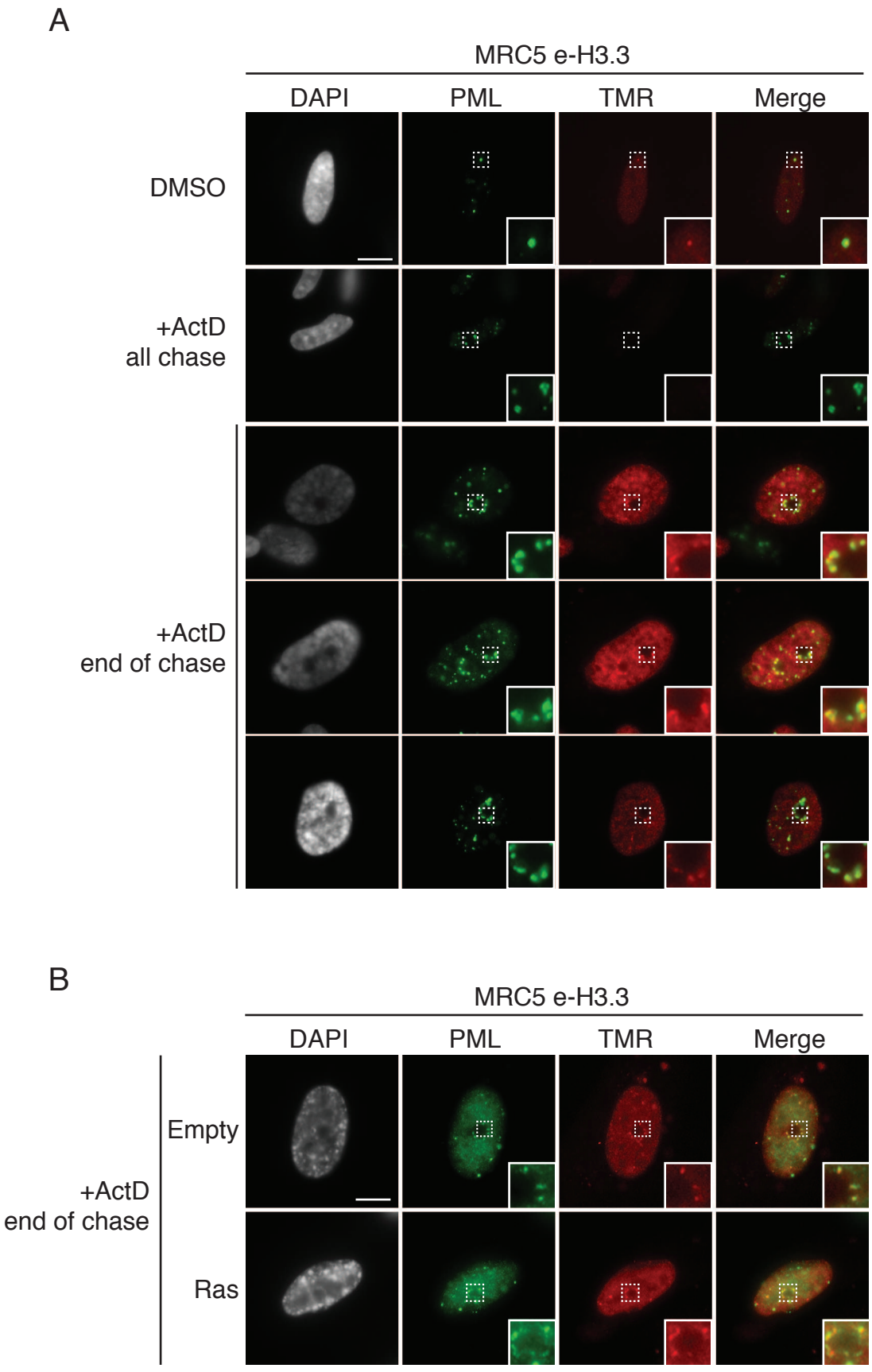

Supplementary Table SI: List of primary antibodies

Antibody	Company/Reference	Order number	Lot number	Species	WB dilution	IF dilution
ASF1a	Mello et al., 2002	#28134	-	Rabbit polyclonal	1/1000	1/1000
α-Tubulin	SIGMA	T6199	-	Mouse monoclonal	1/200	-
ATRX	Santa Cruz Biotechnology	sc-15408 (clone H-300)	F0211	Rabbit polyclonal	1/1000	1/250
Cyclin A	Santa Cruz Biotechnology	sc-751 (clone H-432)	G0811	Rabbit polyclonal	1/1000	-
DAXX	Santa Cruz Biotechnology	sc-7152 (clone M-112)	E1412	Rabbit polyclonal	1/1000	1/250
HA	Abcam	ab9110	-	Rabbit polyclonal	1/6000	1/1000
HIRA	Active Motif	39558 (clone WC119.2H11)	909001	Mouse monoclonal	1/1000	1/100
HP1γ	Pierce - Thermo Scientific	PA5-17445	OB1666806	Rabbit polyclonal	-	1/200
H3.3	Abnova	H00003021-M01 (clone 2D7-H1)	12264-S1	Mouse monoclonal	1/100	1/100
MCM7	Santa Cruz Biotechnology	sc-65469 (clone DCS-141)	H0210	Mouse monoclonal	1/500	-
Myc	GeneTex	GTX80249	-	Mouse monoclonal	1/2000	1/250
PML	Santa Cruz Biotechnology	sc-5621 (clone H-238)	K2912	Rabbit polyclonal	1/500	1/100
PML	Santa Cruz Biotechnology	sc-966 (clone PG-M3)	F1511	Mouse monoclonal	-	1/250
p16	Santa Cruz Biotechnology	sc-56330 (clone JC8)	I2512	Mouse monoclonal	1/200	-
Ras	BD Transduction Laboratories	610001	82593	Mouse monoclonal	1/1000	1/500
Smc1	Abcam	ab9262	GR1468-4	Rabbit polyclonal	1/1000	-
IgG	Santa Cruz Biotechnology	sc-2027	C0411	Rabbit Polyclonal	1μg for IP	-